Cell Reports

Article

Sepsis induces non-classic innate immune memory in granulocytes

Graphical abstract

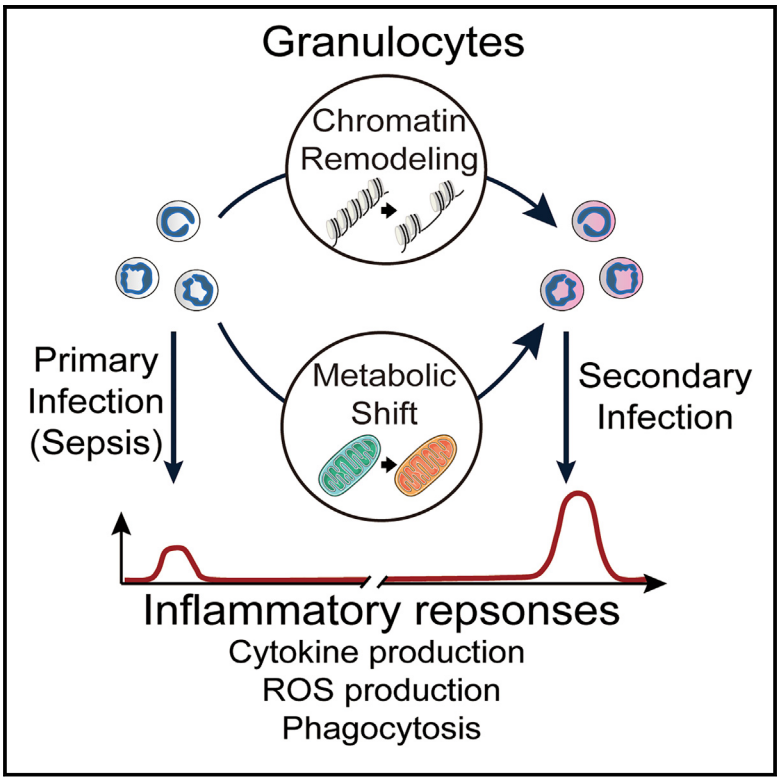

Authors

Beibei Wang, Liuluan Zhu, Bei Jia, ..., Chen Chen, Yaluan Ma, Hui Zeng

Correspondence

yaluanma@yahoo.com (Y.M.), zenghui@ccmu.edu.cn (H.Z.)

In brief

In septic mice, Wang et al. identify stressed granulocytes with innate immune memory. These stressed granulocytes pose an amplified immune response, specifically causing lung injuries and increasing mortality during secondary infections. The study explains how stressed granulocytes determine host fate in secondary infections after sepsis.

Highlights

- Sepsis induces innate immune memory in stressed granulocytes
- Stressed granulocytes boost fatal inflammatory responses to secondary infections
- Chromatin remodeling of the TLR4 pathway and metabolic shift work independently
- Stressed granulocytes specifically target lungs by the CXCL2-CXCR2 axis

Wang et al., 2023, Cell Reports *42*, 113044
September 26, 2023
https://doi.org/10.1016/j.celrep.2023.113044

CellPress

Cell Reports

CellPress
OPEN ACCESS

Article

Sepsis induces non-classic innate immune memory in granulocytes

Beibei Wang,[1,2,10] Liuluan Zhu,[1,2,10] Bei Jia,[1,2,10] Chenchen Zhao,[1,2,10] Ju Zhang,[3,4,10] Fangyuan Li,[3,4] Jiarui Li,[1,2] Nan Ding,[3,4] Can Zhang,[3,4] Yu Hao,[3,4] Shuai Tong,[3,4] Jiajia Wang,[3,4] Guoli Li,[1,2] Yang Fan,[3,4] Henghui Zhang,[3,4] Rui Li,[1,2] Juan Du,[1,2] Yaxian Kong,[1,2] Yue Zhang,[1,2] Xiaoyu Yang,[1,2] Junyan Han,[1,2] Zhengya Yu,[5] Zhongtao Du,[5] Hong Zheng,[6] Christian Kosan,[7] Ang Li,[8] Chen Chen,[3,4] Yaluan Ma,[9,*] and Hui Zeng[3,4,11,*]

[1]Institute of Infectious Diseases, Beijing Ditan Hospital, Capital Medical University, Beijing 100015, China
[2]Beijing Key Laboratory of Emerging Infectious Diseases, Beijing 100015, China
[3]Biomedical Innovation Center, Beijing Shijitan Hospital, Capital Medical University, Beijing 100038, China
[4]Beijing Key Laboratory for Therapeutic Cancer Vaccines, Beijing 100038, China
[5]Department of Vascular Surgery, Beijing Tongren Hospital, Capital Medical University, Beijing 100015, China
[6]Penn State Hershey Cancer Institute, Penn State University College of Medicine, Hershey, PA 17033, USA
[7]Department of Biochemistry, Center for Molecular Biomedicine (CMB), Friedrich- Schiller-University, 07743 Jena, Germany
[8]Intensive Care Unit, Beijing Ditan Hospital, Capital Medical University, Beijing 100015, China
[9]The Institute of Basic Medical Theory of Chinese Medicine, China Academy of Chinese Medical Sciences, Beijing 100700, China
[10]These authors contributed equally
[11]Lead contact
*Correspondence: yaluanma@yahoo.com (Y.M.), zenghui@ccmu.edu.cn (H.Z.)
https://doi.org/10.1016/j.celrep.2023.113044

SUMMARY

Secondary infection in patients with sepsis triggers a new wave of inflammatory response, which aggravates organ injury and increases mortality. Trained immunity boosts a potent and nonspecific response to the secondary challenge and has been considered beneficial for the host. Here, using a murine model of polymicrobial infection, we find that the primary infection reprograms granulocytes to boost enhanced inflammatory responses to the secondary infection, including the excessive production of inflammatory cytokines, respiratory burst, and augmented phagocytosis capacity. However, these reprogramed granulocytes exhibit "non-classic" characteristics of innate immune memory. Two mechanisms are independently involved in the innate immune memory of granulocytes: a metabolic shift in favor of glycolysis and fatty acid synthesis and chromatin remodeling leading to the transcriptional inactivity of genes encoding inhibitors of TLR4-initiated signaling pathways. Counteracting the deleterious effects of stressed granulocytes on anti-infection immunity might provide a strategy to fight secondary infections during sepsis.

INTRODUCTION

Sepsis is a life-threatening organ dysfunction caused by dysregulated host immune responses to infections.[1] Despite recent progress in refining clinical approaches, sepsis is still the leading cause of morbidity and mortality in hospitalized patients and is responsible for more than 5 million deaths worldwide each year.[1–3] Patients with sepsis typically enter a state of immune suppression or even immune paralysis and are predisposed to secondary infections.[4] This secondary infection triggers a new wave of inflammatory responses,[4–6] which aggravates organ injuries and leads to a higher rate of late mortality.[7] Therefore, it is important to investigate how the immune system responds to secondary infections after sepsis.

Unlike adaptive immunity, innate immunity is thought to mount secondary responses without immunological memory.[8] Recent studies on the innate immune memory have challenged this notion,[9–11] imprinting from the primary infection via differentiation and functional remodeling.[12–15] A short pre-exposure to pathogens or pathogen-associated molecular patterns (PAMPs) from microorganisms causes innate immune cells to undergo different adaptive remodeling, manifesting as hyporesponsiveness (tolerance) or hyper-responsiveness (priming or trained immunity).[16] Priming occurs in the innate immune cells whose functional cell status does not return to basal levels and represents an additive or synergistic effect of primary and secondary stimuli.[16] In cells of trained immunity, the functional immune status returns to basal levels after removing the primary stimulus.[16] Trained immune cells are typically subjected to metabolic and chromatin remodeling, such as increased glycolysis, reduced fatty acid metabolites, and active epigenetic histone marks on promoters and distal enhancers.[17] As trained immunity boosts a potent and nonspecific response to the second challenge, it has been considered beneficial for the host to defend against secondary infections.[18,19] Previous studies have investigated trained immunity in monocytes, macrophages, and natural killer cells,[13,20] and recently in β-glucan trained tumor-associated neutrophils (TANs).[21] In these studies, trained immunity is

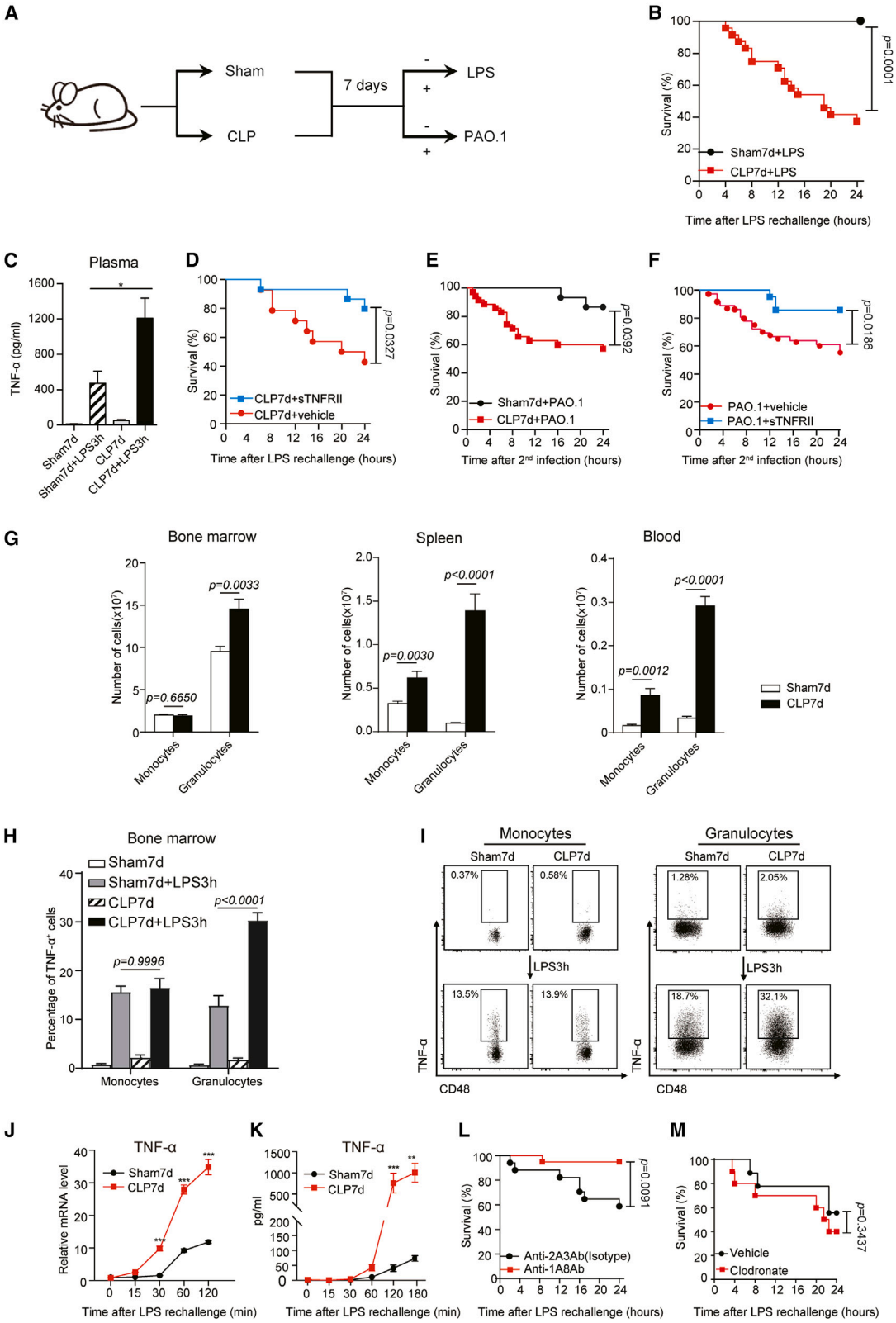

(legend on next page)

induced by transient exposure to a single component from pathogens, a vaccine, or a metabolite.[12,22–24] However, sepsis is a complicated process, in which the innate immune system is under sustained exposure to various components of a pathogen or multiple pathogens throughout the primary infection.[25,26] In addition, as the most abundant circulating leukocytes, granulocytes have a short lifespan. To meet the increased demand for pathogen clearance and compensate for the rapid loss of granulocytes, primary infections could rapidly trigger a process called emergency hematopoiesis.[27] The inflammatory environment related to emergency hematopoiesis can reprogram the differentiation of granulocytes.[27] Therefore, it is important to investigate whether these granulocytes generated under the stressed conditions (proposed as stressed granulocytes) exhibit characteristics related to trained immunity.

In the present study, we used a murine model of polymicrobial infection and a combination of transcriptomic, metabolomic, and functional approaches to demonstrate that emergency-hematopoiesis-derived granulocytes displayed features different from typically trained immunity and posed an amplified immune response during secondary infections.

RESULTS

Excessive TNF-α production during secondary infections in mice with sepsis

C57BL/6J mice were subjected to cecal ligation and puncture (CLP). About half of the mice survived and entered a stable phase until day seven after the CLP operation (CLP7d mice; Figure S1). Mice recovered from the sham operation (Sham7d) were used as controls. To simulate the clinical scenarios of secondary infections after one week of primary infection, Sham7d and CLP7d mice were intraperitoneally (i.p.) injected with low-dose LPS (10 mg/kg) as a secondary challenge (Figure 1A). About 60% of CLP7d mice injected with LPS died within 24 h, whereas all the Sham7d mice survived after the LPS rechallenge (Figure 1B; $p = 0.001$), suggesting that CLP7d mice were hypersensitive to the secondary stimulus. We measured the plasma levels of pro-inflammatory and anti-inflammatory cytokines (Figures 1C and S2). Before LPS rechallenges, the plasma TNF-α, IL-10, IL-12, and IFN-γ in CLP7d mice returned to near basal levels. LPS rechallenge induced significantly higher levels of TNF-α and IL-10 but lower plasma levels of IFN-γ and IL-12 in CLP7d mice than that of Sham7d mice (Figures 1C and S2). The mortality rate of CLP7d mice was significantly reduced by TNF-α neutralization with the i.p. administration of the soluble TNF-α receptor 1 h before the LPS rechallenge (Figure 1D; $p = 0.0327$).

Next, we intranasally administered viable *Pseudomonas aeruginosa* (strain *PAO.1*) to CLP7d mice to simulate secondary infection in respiratory tract.[28] Consistent with LPS-induced secondary infection, CLP7d mice displayed a higher mortality rate than that of control mice within 24 h after infection with *P. aeruginosa* (Figure 1E; $p = 0.0392$). When CLP7d mice were treated with the soluble TNF-α receptor II against TNF-α, the disease was ameliorated, and mortality decreased (Figure 1F; $p = 0.0186$), suggesting that excessive TNF-α production is a crucial mediator leading to the death of these animals during secondary infections.

Granulocytes exhibited enhanced systemic inflammatory responses during secondary infection

To investigate the source of TNF-α during secondary infections, we measured amount of granulocytes and monocytes in bone marrow, spleen, and peripheral blood. Consistent with previous studies about emergency myelopoiesis,[29] granulocytes were the dominant fraction of $CD11b^+$ myeloid cells in CLP7d mice (bone marrow, 87.82% ± 5.16%; spleen, 65.78% ± 14.61%), along with a dramatically increased number of granulocytes in the bone marrow, spleen, and peripheral blood (Figure 1G).

Next, we isolated myeloid cells from Sham7d and CLP7d mice and stimulated them *in vitro* with LPS. Intracellular TNF-α staining revealed that Sham7d and CLP7d mice had similar percentages of $TNF\text{-}\alpha^+$ cells among monocytes from the bone marrow, lungs, spleens, and blood (Figures 1H, 1I, and S3), as well as macrophages from the lungs, the peritoneal cavity, and the liver (Figure S4). In contrast, granulocytes from CLP7d mice exhibited a higher percentage of $TNF\text{-}\alpha^+$ cells than that of Sham7d mice in response to the LPS rechallenge (Figures 1H, 1I, and S3).

Figure 1. Sepsis-induced granulocytes produce excessive TNF-α in response to secondary infection

(A) Proposed mechanism for a mouse model of secondary infection in sepsis.

(B) Survival of Sham7d and CLP7d mice challenged with LPS (10 mg/kg). Sham7d+LPS3h, n = 16; CLP7d+LPS3h, n = 25.

(C) Concentrations of TNF-α in peripheral blood, as measured using a cytometric bead array. Sham7d, n = 3; Sham7d+LPS3h, n = 7; CLP7d, n = 5; CLP7d+LPS3h, n = 7.

(D) Protective effect of blocking TNF-α. An anti-TNF-α reagent was administered 18 h before and 1 h after LPS (10 mg/kg) injection into CLP7d mice. Vehicle, n = 14; TNF-α inhibitor, n = 15.

(E) Survival of Sham7d, CLP7d mice with intranasal *P. aeruginosa* infection. For each group, n = 20.

(F) Protective effect of TNF-α receptor blockade in CLP7d mice with secondary *P. aeruginosa* infection (n = 21).

(G) Absolute number of granulocytes and monocytes in bone marrow (left), spleen (middle), and blood (right) 7 days after the CLP procedure. Sham7d, n = 18; CLP7d, n = 24.

(H) Intracellular staining of TNF-α protein in granulocytes and monocytes from each group. Sham7d, n = 3; Sham7d+LPS3h, n = 7; CLP7d, n = 5; CLP7d+LPS3h, n = 7.

(I) Representative flow cytometry dot plots of the $TNF\text{-}\alpha^+$ ratio in granulocytes and monocytes.

(J) TNF-α mRNA expression in granulocytes isolated from the bone marrow of each group and stimulated by LPS (100 ng/mL).

(K) TNF-α secretion level in granulocytes isolated from the bone marrow of each group and stimulated by LPS (100 ng/mL).

(L) Survival rate of LPS-induced secondary infection in sepsis after granulocyte depletion with an anti-1A8 antibody. Anti-1A8 antibody, n = 20; anti-2A3 negative control antibody, n = 17.

(M) Survival rate of LPS-induced secondary infection in sepsis after monocyte/macrophage depletion with clodronate. Vehicle, n = 10; clodronate, n = 10.

*$p < 0.05$, **$p < 0.01$, and ***$p < 0.001$ (two-tailed unpaired t test). For each bar graph, the bar indicates the mean ± SEM.

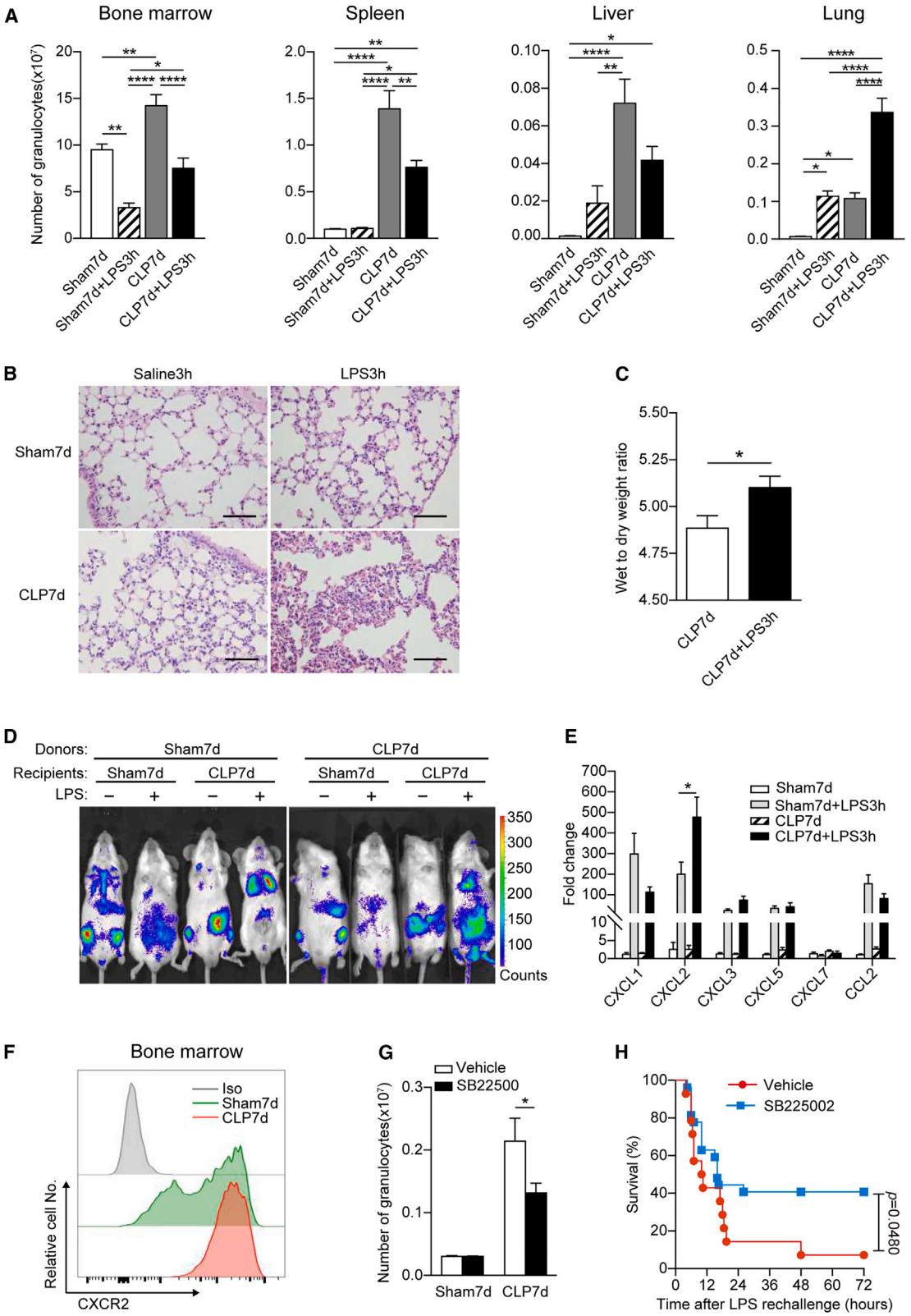

(legend on next page)

Consistently, granulocytes from CLP7d mice expressed higher levels of TNF-α mRNA (Figure 1J) and released significantly higher amounts of TNF-α protein in the culture medium (Figure 1K). We further depleted granulocytes in CLP7d mice with an anti-Ly6G antibody (clone 1A8) or depleted monocytes/macrophages with clodronate. The mortality rate induced by the LPS rechallenge was reduced by the anti-Ly6G antibody (Figure 1L) but not clodronate treatment (Figures 1M and S5). Therefore, the data suggest that granulocytes are the major cell compartment which contributes to overwhelming inflammatory response during secondary infections.

Granulocytes specifically targeted lungs during secondary infection

We further assessed the target organ of granulocytes during secondary infections. After three hours of LPS stimulation, the numbers of granulocytes dramatically decreased in the bone marrow, spleen, and liver (Figure 2A) but significantly increased in the lungs of CLP7d mice (Figure 2A). High levels of granulocyte infiltration were observed in the intra-alveolar and interstitial spaces of the lung, along with a thickened alveolar interstitium, partial alveolar atelectasis, and increased wet-to-dry weight ratios (Figures 2B and 2C). These data suggest that the lungs are a key target organ of sepsis-trained granulocytes during secondary infections.

Next, we performed cross-adoptive transfer experiments and illustrated the influx of granulocytes into the lungs with *in vivo* bioluminescence imaging. Donor granulocytes from either Sham7d or CLP7d mice primarily settled at the site of hematopoiesis and lymphoid organs (the sternum, ribs, spleen, and lymph nodes) of Sham7d recipients and predominantly in the abdominal cavity of CLP7d recipients (Figure 2D). When the recipients were subjected to the i.p. injection of LPS, donor granulocytes migrated to the abdominal cavity (Figure 2D). Strikingly, donor granulocytes also migrated to the lungs of CLP7d recipients, regardless of which donors these cells were isolated from (Figure 2D). These data suggest that CLP-induced intrapulmonary mechanisms are responsible for recruiting granulocytes to the lungs during secondary infections.

We further assessed the mRNA abundance of several chemokines in lung homogenates using real-time PCR. Compared with Sham7d mice, CLP7d mice exhibited a significant elevation of transcripts of CXCL2 after LPS stimulation (Figure 2E). Consistent with previous studies,[30–32] single-cell transcriptome analysis revealed CXCL2 signals in the type 2 alveolar epithelial cells (AT2), granulocytes, and monocytes (Figure S6). Meanwhile, granulocytes from CLP7d mice expressed higher levels of CXCR2, the receptor for CXCL2 (Figure 2F). In support of this finding, administration of CXCR2 inhibitor SB225002 to CLP7d mice before the secondary challenge significantly reduced the responsive influx of granulocytes into the lungs (Figure 2G) and decreased the LPS-induced mortality rate (Figure 2H). Therefore, the CXCL2-CXCR2 axis might contribute to the recruitment of granulocytes to the lungs during secondary infections.

Innate immune memory in immature and mature granulocytes

As mature granulocytes have short lifespans,[33] we speculated that the capacity for TNF-α production is enhanced during granulocyte differentiation. Therefore, we sorted Lin^- cells that contained hematopoietic progenitor and precursor cells from the bone marrow of C57/B6 mice, then cultured these cells on OP9 stromal cells in the presence of the TLR agonists LPS, Pam3CSK4, and poly(I:C) for seven days to generate differentiated granulocytes and monocytes/macrophages. LPS rechallenge induced higher frequencies of TNF-α^+ cells in the LPS or Pam3CSK4 pre-stimulated granulocytes but not in monocytes/macrophages (Figure 3A).

Since granulocytes are a heterogeneous population, we compared the capacities of TNF-α production in immature and mature granulocytes. According to our previous report,[34] the granulocytes were subdivided into three fractions: immature G1 granulocytes (containing more myelocytes, metamyelocytes, and ring-shaped granulocytes) and relatively mature G2 and G3 granulocytes (containing more banded and segmented granulocytes) (Figures 3B and 3C). CLP7d mice had higher absolute numbers of all three fractions in the bone marrow, spleen, and lungs (Figure 3D). All three granulocyte fractions from CLP7d mice produced greater amounts of TNF-α compared with granulocytes from control mice (Figure 3E). Notably, more mature G3 granulocytes had a higher capacity to produce TNF-α than relatively immature G1 and G2 fractions. In addition, we tested the capacities of phagocytosis and respiratory burst, which are essential for granulocytes to eliminate bacteria. Compared with granulocytes from Sham7d mice, G3 granulocytes from CLP7d mice displayed significant increases in respiratory burst (Figure S7A). G1 and G2 granulocytes from CLP7d mice showed a slightly higher phagocytic ability (Figure S7B).

Polymicrobial infection affects the trajectory of inflammation but not granulocyte differentiation

To test whether polymicrobial infection affects granulocyte differentiation, we performed single-cell RNA sequencing (scRNA-seq)

Figure 2. Secondary infection-induced granulocytes are involved in acute lung injury during secondary infections

(A) Absolute number of granulocytes in the bone marrow, spleen, liver, and lung of each group of mice. Sham7d, n = 18; Sham7d+LPS3h, n = 13; CLP7d, n = 24; CLP7d+LPS3h, n = 21.

(B) Representative images (H&E staining) of lung histopathology. Scale bars, 200 μm.

(C) Wet-to-dry ratio of lungs of CLP7d mice with and without LPS challenge. For each group, n = 5.

(D) *In vivo* imaging of mice transplanted with granulocytes from luciferase mice (n = 5).

(E) qPCR analysis of CXCL1/2/3/5/7 and CCL2 transcripts in the lungs of mice from each group. GAPDH was selected as the housekeeping control. Fold change is relative to CXCL1 in Sham7d mice. For each group, n = 5.

(F) Representative histogram of CXCR2 expression on granulocytes from Sham7d or CLP7d mice.

(G) Number of granulocytes in the lungs after SB225002 (2 mg/kg) was used as a CXCR2 inhibitor in CLP7d mice challenged with LPS. For each group, n = 3.

(H) Survival of CLP7d mice rescued by the administration of SB225002 during secondary LPS challenge. Vehicle, n = 14; SB225002, n = 27.

*p < 0.05, **p < 0.01, and ****p < 0.0001 (two-tailed unpaired t test or ANOVA). For each column plot, the bar indicates the mean ± SEM.

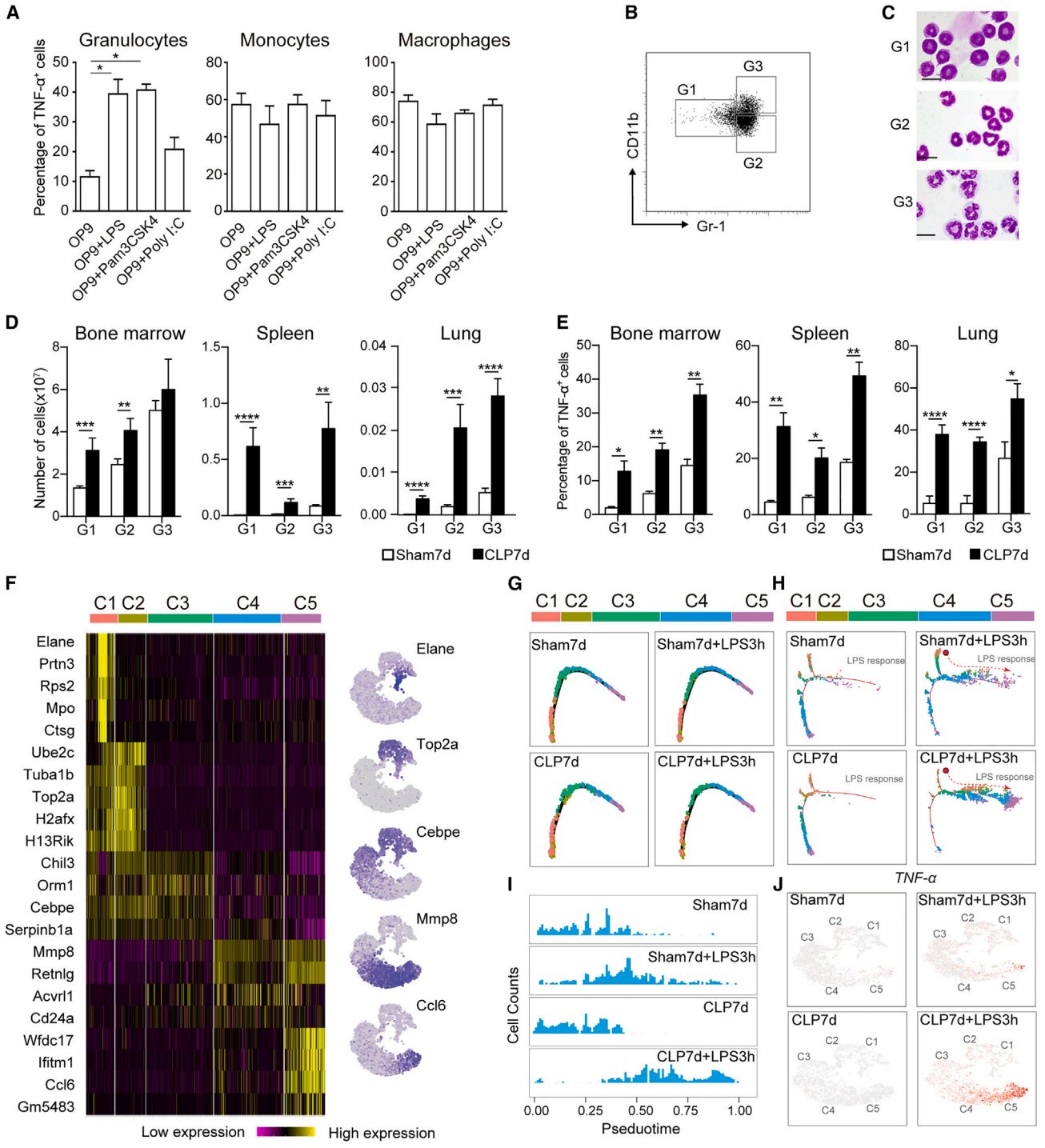

Figure 3. Trained immunity from progenitor cells to mature granulocytes

(A) Percentage of TNF-α^+ cells in granulocytes, monocytes, and macrophages stimulated by different TLR agonists when cocultured with OP9 cells, n = 10.

(B) Flow cytometry dot plots showing the gating strategy of the three subsets (G1, G2, and G3) of granulocytes from mice with the sham CLP operation.

(C) Giemsa staining graph of subsets of granulocytes from mice with the sham CLP operation.

(D and E) Absolute number counts (D) and intracellular staining of TNF-α protein (E) in the G1, G2, and G3 subsets of the bone marrow, spleen, and lung of each group of mice. Sham7d, n = 18; CLP7d, n = 12.

(F) Differentially expressed genes (DEGs) in 5 cell clusters of cells divided by scRNA-seq. Heatmap represents the top 5 gene transcripts for each cell cluster (C2 and C3 only have 4 DEGs that met the criteria, and overlapped genes were removed). uniform manifold approximation and projection (UMAP) highlighted the expression level of five major genes indexed the differentiations.

(legend continued on next page)

on granulocytes from Sham7d and CLP7d mice. After removing low-quality sequencing data, cells with expressed gene counts between 200 and 7,600 were included in subsequent analyses (Table S1). Following data normalization, an unsupervised graph-based clustering algorithm was performed to divide all qualified cells into five groups (C1–C5) (Figure S8). In total, we observed 921 (619, 227, 4, 4, and 67 in each cluster) differentially expressed genes (DEGs) by pairwise comparisons. The most significant DEGs in each group were visualized using a heatmap (Figure 3F, left). Five marker genes (*Elane*, *Top2a*, and *Cebpe* are down-regulated during differentiation, and *Mmp8* and *Ccl6* are highly expressed in terminally differentiated granulocytes 33[35] and were highlighted and indexed in the different stages of granulocyte maturation (Figure 3F, right). Next, we performed differentiation trajectory analysis of granulocytes from Sham7d and CLP7d mice. Using the 921 DEGs identified in each cluster, we found that granulocytes in CLP7d mice displayed a similar differentiation trajectory to Sham7d mice regardless of LPS rechallenge (Figure 3G).

We also measured the trajectory inference of LPS secondary stimulation. Using 245 genes that were significantly up-regulated in response to LPS stimulation (Table S2), the trajectory analysis showed that the LPS challenge shifted more cells toward LPS-response trajectory in both Sham7d and CLP7d mice (Figure 3H). More granulocytes were observed in the terminal stage of the trajectory in LPS rechallenged CLP7d mice (Figures 3H and 3I), suggesting an enhanced response to LPS. Consistently, higher TNF-α^+ cell levels were detected in more mature granulocytes in response to the LPS rechallenge in CLP7d mice (Figure 3J). All of these observations indicated that polymicrobial infection affects cell distributions along the trajectory of inflammation instead of granulocyte differentiation.

Transcriptome and epigenetic reprogramming in stressed granulocytes

To gain more insight into the mechanism of excessive TNF-α production in granulocytes, we performed bulk RNA sequencing analyses of three granulocyte subpopulations (G1, G2, and G3, previously defined) along the granulocyte differentiation path. We obtained 84.17 G RNA sequencing data, and 11,863 genes were detected (fragments per kilobase of exon per million reads mapped [FPKM] > 1 in at least two samples). Of them, 1,078 DEGs (737 were up-regulated, and 339 were down-regulated) were identified in CLP7d granulocytes (Figure 4A; Table S3). Among granulocyte subsets, the G3 subset had 76% (819 of 1,078) of total DEGs and exhibited the lowest similarity (R^2 = 0.886) in expression profiles between cells from CLP7d and Sham7d mice (Figures 4A and 4B). We performed a functional analysis on the basis of DAVID (Database for Annotation, Visualization, and Integrated Discovery)[36] and found that DEGs were enriched in the metabolic and immune system processes in all three granulocyte subsets (Figure 4C; Tables S4 and S5), but especially in the G3 subset. As such, the G3 subset dominated the response module of immune memory, which is consistent with the high capacity of TNF-α production (Figure 3E).

The further biological pathway analysis with gene set enrichment analysis (GSEA)[37] revealed that DEGs in G3 were primarily enriched in the metabolic pathway (carbon metabolism), Toll-like receptor (TLR) signaling pathway, and NF-κB signaling pathway in CLP7d granulocytes (Figure 4D). According to the weight of expressed genes, we scored the DEGs of these pathways in each group. Compared with G1 and G2 granulocytes, G3 had higher carbon metabolism scores (Figure 4E), fatty acid metabolic (Figure 4F) and pro-inflammatory effects (Figure 4G). When mapping the DEGs responsible for pro-inflammatory effects in the signaling network, the TLR4 signaling and its downstream MAPK and NF-κB pathways were enriched after the secondary challenge of LPS (Figure 4H; Table S6). Consistently, western blot demonstrated enhanced phosphorylation of MAPK p38 (Figure 4I), as well as more rapid phosphorylation of NF-κB p65 subunit in the granulocytes from CLP7d mice (Figure 4I), confirming the hyperactivation of TLR4 downstream signaling pathways.

To examine whether the enhanced inflammatory profiles in CLP7d granulocytes accompanied with epigenetic reprogramming, we conducted assay for transposase-accessible chromatin with high-throughput sequencing (ATAC-seq). A total of 43,250 ATAC-seq peaks were detected in the granulocytes of Sham7d and CLP7d. Out of these peaks, 14.11% (n = 6,102) had undergone dynamic changes during sepsis and secondary infections. Compared with the granulocytes from Sham7d mice, CLP7d granulocytes had 1,056 genomic regions that had gained accessibility, with only 15 genomic regions being closed off (Figure 5A). We further traced histone marks on these genomic regions with Cut&Run experiments,[38] and found a significant increase in H3K27ac levels and a decrease in H3K4me2 levels in the CLP7d granulocytes, either with or without the secondary challenge (Figure 5B). The H3K9ac levels showed an overall decrease in CLP7d mice in a LPS-susceptible manner (Figure 5B). Taken together, the stressed granulocytes are subjected to genome-wide epigenetic remodeling. Consistent with the transcriptomic data, the accessible genomic regions in CLP7d granulocytes were concentrated in pathways associated with the immune processes, including TLR signaling pathways and its downstream MAPK and NF-κB signaling (Figures 5C and 5D; Table S7). It demonstrated that the epigenetic remodeling is related to enhanced inflammatory responses to the secondary infection.

(G) Single-cell distribution along pseudotime trajectory by 921 DEGs pairwise compared in each cluster, indexed the differentiation stages in the Sham7d, Sham7d+LPS3h, CLP7d, and CLP7d+LPS3h groups.

(H) Single-cell distribution along pseudotime trajectory by DEGs related to LPS-stimulated responses indexed the differentiation stages in the Sham7d, Sham7d+LPS3h, CLP7d, and CLP7d+LPS3h groups.

(I) Differential cell counts along pseudotime trajectory by LPS-stimulated responses related genes in the Sham7d, Sham7d+LPS3h, CLP7d, and CLP7d+LPS3h groups.

(J) Single-cell expression level of TNF-α in the Sham7d, Sham7d+LPS3h, CLP7d, and CLP7d+LPS3h groups.

*p < 0.05, **p < 0.01, ***p < 0.001, and ****p < 0.0001 (two-tailed unpaired t test). For each column plot, the bar indicates the mean ± SEM.

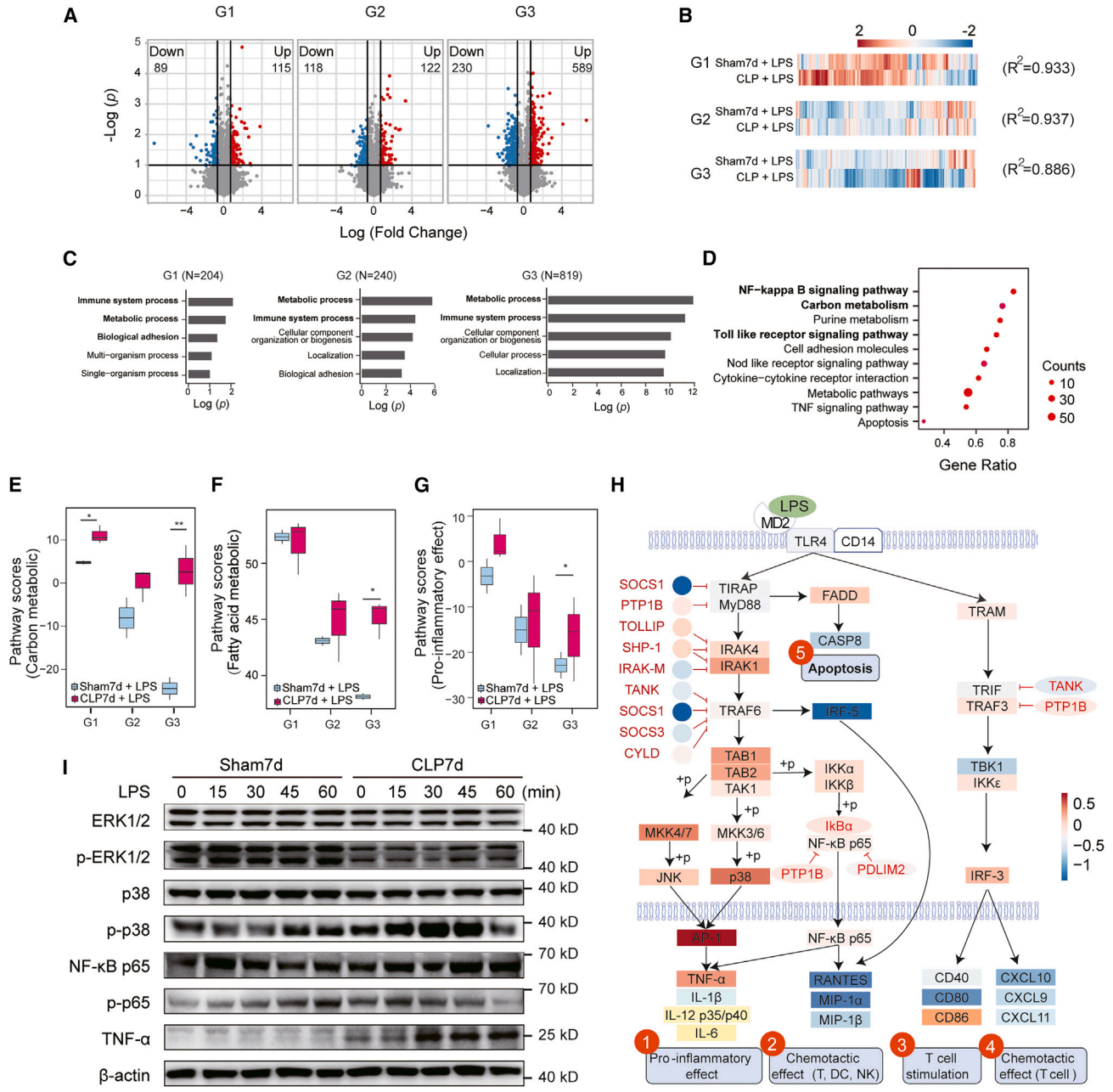

Figure 4. Different expressions of genes are affected by CLP training

(A) Volcano plot of differential expression genes in the LPS-treated G1, G2, and G3 granulocytes from CLP7d (CLP7d+LPS) and Sham7d mice (Sham7d+LPS). Significantly expressed genes with a fold change above or below 2-fold and p value less than 0.1 are highlighted with blue and red.

(B) Two-dimensional hierarchical clustering of genes expressed in granulocytes treated by LPS and CLP-LPS. Expression levels have been scaled according to the expression level in each sample. The heatmap represents the lg-transformed fold change in the expression level. The correlations of expression levels in G1, G2, and G3 were calculated on a linear model.

(C) Gene Ontology (GO) biological process terms enriched in up- and down-regulated gene groups in the three cell groups on the basis of separate DAVID ontology analysis. N, number of genes enriched in each dataset. The length of the bar for the BP relates to the $-\log_{10}$ (p value).

(D) GSEA shows biological pathway enrichment of G3.

(E–G) Scores of DEG enrichment in carbon metabolism (E), fatty acid metabolitic (F) and pro-inflammatory effects (G). Functional scores were measured by the normalized expression of corresponding genes and gene weight, where gene weights were set to either 1 or −1 to reflect positive or negative relationships.

(legend continued on next page)

Stressed granulocytes with downregulation of negative regulators of the TLR4 signaling pathway

To investigate the critical regulators of the TLR4 pathway, we validated gene expressions that changed in response to secondary infections in RNA sequencing data. Two negative regulators of the TLR4 pathway, Socs1, and Irak3, were on the top list of down-regulated genes (Figure 6A). Real-time PCR and western blot assays confirmed the decreased expression of Socs1 and Irak3 (Figures 6B and 6C).

However, in the CLP7d mice before the secondary stimulus, chromatin immunoprecipitation (ChIP)-PCR assays against TNF-α, Socs1, and Irak3 promoter did not detect significant changes in the essential epigenetic marks (Figure 6D). After the secondary stimulus, H3K27ac and H3K9ac decreased in the promoters of Socs1 and Irak3 genes and increased in the TNF-α promoter (Figure 6D). H3K4me2 remained stable in all detected genomic regions (Figure 6D). We further treated CLP7d granulocytes with suberoylanilide hydroxamic acid (SAHA), a pan-HDAC inhibitor (HDACi) used in the clinic. SAHA pretreatment increased SOCS1 (encoded by Socs1) and IRAK-M (encoded by Irak3) expression levels in CLP7d granulocytes (Figure 6E). Accordingly, the *in vivo* administration of SAHA to CLP7d mice also significantly reduced serum concentrations of TNF-α in response to the secondary LPS challenge (Figure 6F) and improved the survival rate of CLP7d mice (Figure 6G).

Metabolic shifts involved in innate immune memory of granulocytes

As the metabolic process was also observed during functional analysis (Figure 4C), we analyzed metabolomes of granulocytes from Sham7d and CLP7d mice. Granulocytes from CLP7d and Sham7d mice had 249 cellular metabolites and displayed different metabolite profiles, as illustrated by partial least square discriminant analysis (PLS-DA; Figure 7A). Notably, both carbohydrate and lipid metabolites was significantly changed in CLP7d granulocytes (Figures 7B and 7C; Table S8). In contrast to carbohydrates increasing or decreasing in stressed granulocytes, most species of fatty acids increased after sepsis (Figure S9A; Table S8).

We measured the extracellular acidification rate (ECAR) and oxygen consumption rate (OCR) in live cells with a Seahorse XF Analyzer. In CLP7d granulocytes, aerobic glycolysis and oxidative phosphorylation were both enhanced (Figures 7D and S9B). CLP7d granulocytes displayed a 12-fold increase in glucose-6-phosphate (G6P), an essential metabolic intermediate of glycolysis, and a significantly increased ratio of G6P to D-glucose (Figure 7E). In addition, the intermediate of the second step of the citric acid cycle, isocitrate, also increased by almost 2-fold in CLP7d granulocytes (Figure 7E). We then tested the effects of metabolic inhibitors on the inflammatory responses of CLP7d granulocytes. Both aerobic respiration inhibitors (oligomycin A and antimycin A/rotenone) and the pentose phosphate pathway inhibitor dehydroepiandrosterone (DHEA) failed to prevent excessive TNF-α production (Figure 7F). In contrast, the glycolysis inhibitor 2-deoxyglucose (2-DG) and galloflavin (GF) significantly reduced TNF-α production and respiratory burst without affecting the phagocytotic capacity of these cells (Figure 7F).

As most fatty acids increased in CLP7d mice (Figure S9A), we next tested the effects of the adipose triglyceride lipase inhibitor atglistatin (Atg; which blocks fatty acid mobilization), the cholesterol esterase inhibitor diethylumbelliferyl phosphate (DEUP; which blocks steroidogenesis), or the specific inhibitor of fatty acid synthase (C75) on stressed granulocytes. Only C75 dramatically impaired TNF-α production, respiratory burst, and phagocytosis in stressed granulocytes (Figure 7G). To further confirm the above *in vitro* results, we administrated 2-DG or C75 to the CLP7d mice before the secondary challenge. Consistent with *in vitro* data, 2-DG and C75 significantly reduced the mortality caused by the LPS rechallenge (Figure 7H), and showed promising results in rescuing PAO.1 re-infected mice (Figures S10A and S10B). These results indicate that impaired glycolysis and fatty acid synthesis could hinder the innate immune responses induced by stressed granulocytes.

As both the modification of histone acetylation and metabolic shifts regulated stressed immunity in granulocytes, we further assessed whether these processes influenced each other. Strikingly, SAHA did not temper glycolysis in stressed granulocytes (Figure 7I); inhibitors of glycolysis (2-DG and GF) or fatty acid synthesis (C75) also failed to restore the expression of genes encoding Socs1 and Irak3 genes (Figure 7J). Therefore, intracellular metabolism and epigenetic remodeling seemed to regulate the stressed immunity of granulocytes independently.

DISCUSSION

Polymicrobial infections are common primary infections, which means that innate immune cells have been exposed to multiple and complex microbial components from various pathogens.[25] In this study, we demonstrated that during polymicrobial infection, granulocytes display non-classic traits of innate immunity memory, as defined by increased robust responsiveness to reinfection, including excessive TNF-α production in response to rechallenge with pathogens and an enhanced capacity for phagocytosis and reactive oxygen species (ROS) production. Considering that granulocytes are the most abundant circulating leukocytes in healthy adults and could be greater because of emergency granulopoiesis after primary infections,[29] these changes in the immune function of stressed granulocytes highlight their role during secondary infection in sepsis.

Of note, we demonstrated that polymicrobial infections induced a process of innate immune memory distinct from "priming" and "trained immunity" in granulocytes. Trained immunity and priming are two immunological processes that

(H) Schematic representation of gene pathways involved in the TLR4 pathway on the basis of RNA sequencing (RNA-seq) expression signatures. Five pathways are indicated, as indicated at the bottom and in Table S6. The circle and box color of genes indicates changes of LPS and CLP-LPS expression, respectively. Red line and red gene name indicate negative regulation.

(I) Western blot showing increased TNF-α, phosphorylated p38 (15–45 min), and p65 (0–30 min) in granulocytes from the bone marrow of CLP7d compared with Sham7d mice.

*p < 0.05, **p < 0.01, ***p < 0.001, and ****p < 0.0001 (two-tailed unpaired t test). For each column plot, the bar indicates the mean ± SEM.

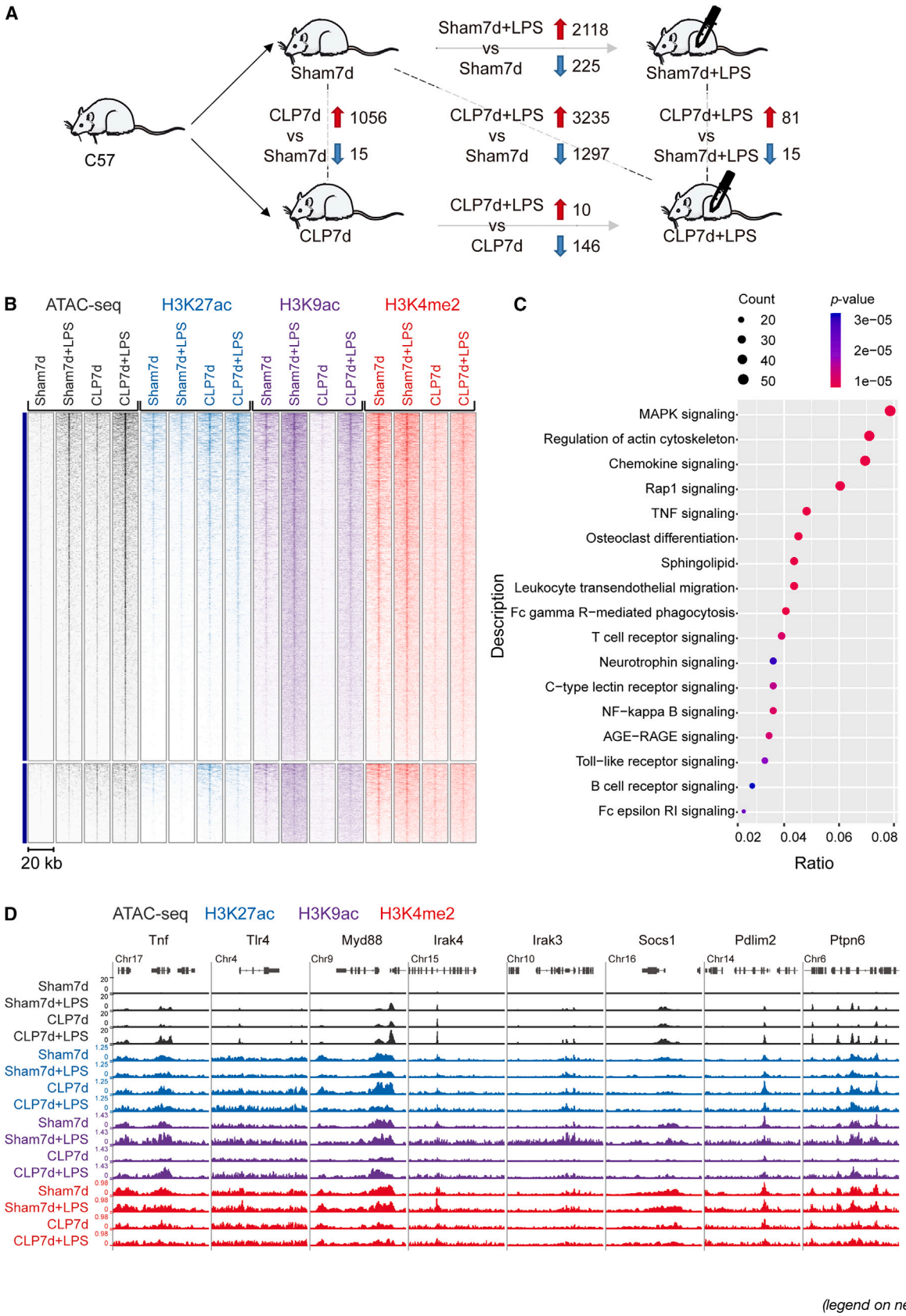

(legend on next page)

display an enhanced functional alternation in response to the secondary stimulus.[10,16] In "trained immunity," the functional immune status returns to basal levels after the primary stimulus, while epigenetic alterations persist in developing enhanced responses upon reinfection.[12,16,39–42] In contrast, "priming" is based on enhanced basal levels of immune status before the secondary stimulus.[16] In this study, we observed that TNF-α expression levels in granulocytes returned to a level close to the baseline with the recovery from CLP7d. The plasma levels of some cytokines (such as IFN-γ) in the secondary stimulation were even lower than those in the primary infections. Therefore, enhanced immune responses in "stressed granulocytes" could not be explained by an additive or synergistic effect of primary and secondary stimuli. In addition, stressed granulocytes in CLP7d mice exhibited different characteristics from "trained immunity." First, CLP7d mice still exhibited low but detectable levels of TNF-α, which were not restored. Second, after removing the primary stimulus, trained immunity exhibited epigenetic reprogramming on numerous pro-inflammatory cytokine genes and lineage-specific genes.[12,18] However, increased H3K27ac and H3K9ac of the TNF-α promoter were observed after, rather than before, the secondary stimulus in granulocytes. Third, metabolic and epigenetic alterations are frequently intertwined in trained immunity,[17] while the glycolysis, fatty acid synthesis, and HDAC all independently executed key functions in granulocytes undergoing "stressed immunity" in mice with polymicrobial infection. Fourth, trained macrophages could be derived from either monocytes or myeloid progenitors,[20] while stressed granulocytes are generated mainly from myeloid progenitors because of their short lifespan. Finally, stressed granulocytes after sepsis exhibit distinguishing characteristics from β-glucan-trained TANs.[21] Trained TANs undergo extensive epigenomic reprogramming, up-regulate their oxidative phosphorylation, and thus promote anti-tumor activities in a ROS-dependent manner. Stressed granulocytes undergo more extensive metabolic rewiring without observable epigenomic marks before the second challenge, and also mediate hyper-inflammatory responses in a TNF-dependent manner.

Cell differentiation trajectory analysis indicated that polymicrobial infections amplify inflammatory responses without shifting granulocytic differentiation. However, mature granulocytes displayed more predominant features of stressed immunity than that of immature granulocytes. This raises a fundamental question about whether stressed immunity can last for longer. In monocytes/macrophages, trained immunity occurs either at the level of mature cells or progenitor cells in the bone marrow. The trained progenitors could be transferred to mature monocyte descendants.[35,43] Unlike monocytes/macrophages, mature granulocytes have short lifespans,[33] meaning that innate immunity memory should occur during the early stages of granulocyte differentiation. This speculation is supported by successfully generating stressed granulocytes from *in vitro* cultured hematopoietic progenitors in the presence of TLR agonists.

As granulocytes with innate immune memory have enhanced capacities of bacterial clearance and cytokine production, theoretically, they may act as a double-edged sword for the patients with sepsis. From the view of eradicating pathogens, a potent innate immune response is in favor of the patients with sepsis. Consistently, we found that either *in vivo* depletion of granulocytes or prevention of granulocytes migration into the lungs failed to rescue mice from rechallenge with *P. aeruginosa* (Figures S10C and S10D). However, CLP7d granulocytes also exhibited typical characteristics of myeloid-derived suppressor cells (Figure S11), which are capable of impairing adaptive immunity.[34,44,45] Therefore, stressed granulocytes could even increase the risk for secondary infections. Once pathogens break through the immune systems and trigger secondary infections, detrimental effects are dominant in stressed granulocytes. From the view of tissue injury, the overwhelming production of inflammatory cytokines by stressed granulocytes are unfavorable, and even lethal, for the hosts. Even worse, the lungs prioritize attracting stressed granulocytes, which further aggravate acute lung injury, even in extrapulmonary infections. It is worth pointing out that the above features of stressed granulocytes are consistent with the complicated status observed in patients with severe infections, including a correlation between elevated neutrophil numbers and poor outcomes in patients with sepsis, a phase termed mixed pro-inflammatory and anti-inflammatory syndrome (MARS), in which a new wave of cytokine storm and a high frequency of acute lung injury occur during secondary infection.[46]

Considering that secondary infections usually occur one week after primary infections,[47] this could present an opportunity to counteract the potentially deleterious effects of stressed granulocytes. As directly purging granulocytes may indiscriminately harms the innate immune responses and impedes bacterial clearance, it is not an option for clinic therapy. It is more conceivable to propose therapeutic approaches for four potential targets: (1) directly neutralizing inflammatory cytokines with blocking antibodies or soluble receptors, (2) minimizing tissue injury with organ-specific chemokine inhibitors, (3) altering the epigenetic landscape with pharmacologic means such as HDACi, and (4) reducing excessive cytokine production by shifting metabolic programs.

Altogether, our study presents insights into the host defense mechanisms during sepsis caused by polymicrobial infection and explains how trained granulocytes determine host fate in response to secondary infections.

Figure 5. Epigenetic remodeling are involved in the innate immunity memory of granulocytes

(A) Scheme of ATAC-seq assays and numbers of genomic regions with differential chromatin accessibility between granulocytes from the Sham7d, Sham7d+LPS3h, CLP7d, and CLP7d+LPS3h groups.

(B) Pile-up heatmap of genomic regions achieving accessibility (±10 kb around the center of those peaks) in CLP7d granulocytes and the corresponding H3K27ac, H3K9ac, and H3K4me2 epigenetic marks.

(C) Kyoto Encyclopedia of Genes and Genomes (KEGG) pathway enriched from genes around genomic regions achieving accessibility in CLP7d granulocytes. Dots determined by count of genes enriched in pathways (size) and significance (color), columns showing ratios of enriched genes of total genes from KEGG pathways.

(D) Screen shots of the accessible genomic regions and epigenetic landscape at representative gene loci corresponding to TLR signaling pathway.

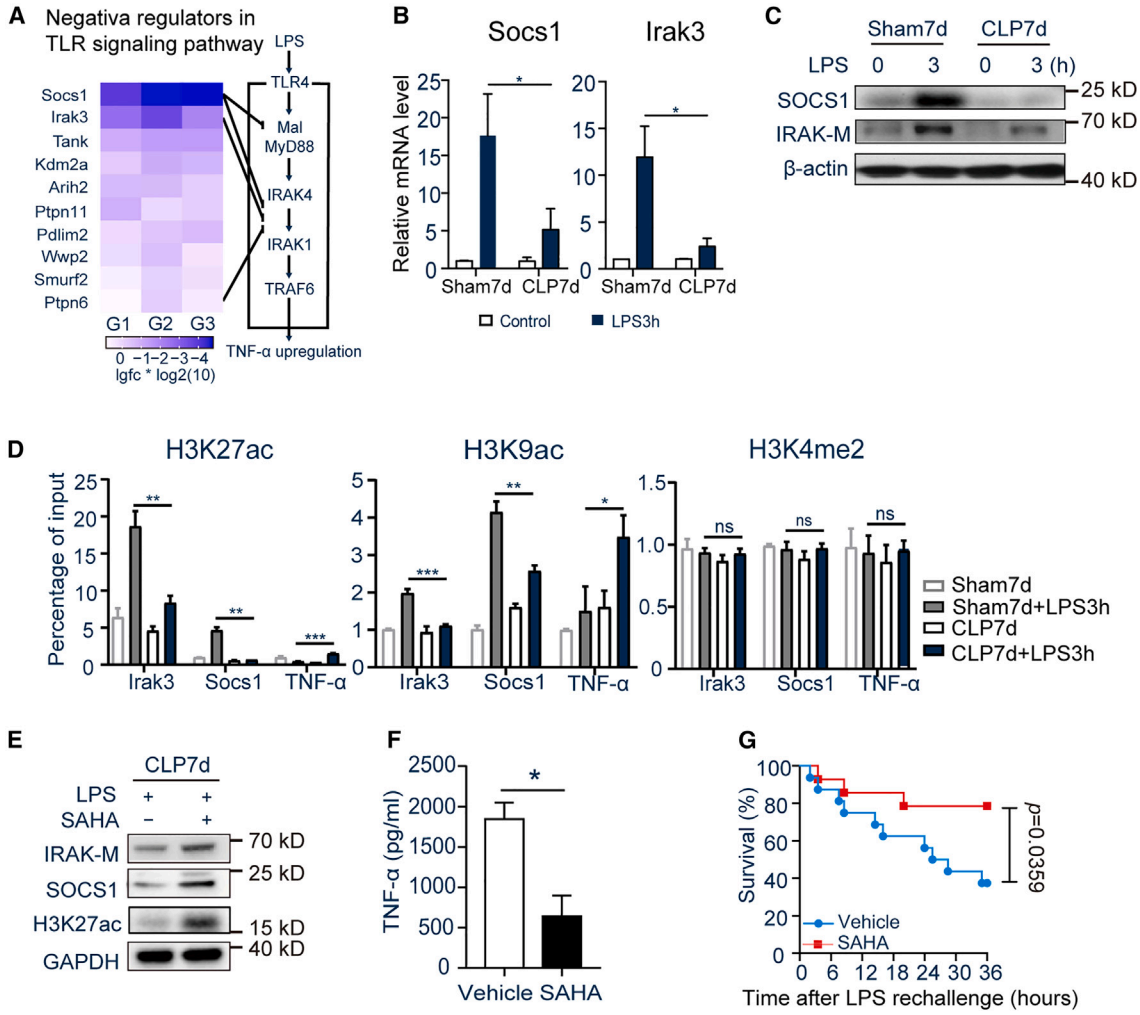

Figure 6. The increased expression of TNF-α and decreased expression of negative regulators of the TLR4 signaling pathway in trained granulocytes are associated with chromatin acetylation

(A) Expression changes of negative regulators of the TLR signaling pathway in CLP-treated granulocytes after exposure to LPS. The left heatmap represents the log2-transformed fold change in the expression level of negative regulatory genes in CLP7d granulocytes exposed to LPS compared with those in Sham7d granulocytes exposed to LPS.

(B and C) qRT-PCR analysis of *Socs1* and *Irak3* transcripts (B) and western blot analysis of their corresponding proteins (C) expressed by granulocytes from the bone marrow of CLP7d mice with a 3 h LPS (100 ng/mL) challenge *in vitro*. The experiments were performed with three independent replicates per group.

(D) ChIP-PCR analysis showing histone modification status in the promoter region of the genes *Socs1*, *Irak3*, and *TNF-α*. The acetylation of H3K27 and H3K9 and the methylation of H3K4 were examined in isolated bone marrow granulocytes. The experiments were performed with three independent replicates per group.

(E) Western blot of IRAK-M, SOCS1, and total H3K27Ac in LPS-stimulated granulocytes with and without SAHA treatment *in vitro*. The experiments were performed with three independent replicates per group.

(F) Plasma levels of TNF-α at 3 h after the secondary LPS challenge of CLP7d mice that were rescued by SAHA. Vehicle, n = 4; SAHA, n = 5.

(G) Survival curve showing the protective effects of SAHA in the secondary LPS challenge of CLP7d mice. Vehicle, n = 16; SAHA, n = 14.

*p < 0.05, **p < 0.01, and ****p < 0.0001 (two-tailed unpaired t test or ANOVA). For each column plot, the bar indicates the mean ± SEM.

Limitations of the study

The present study is limited to a rodent model of polymicrobial infection. To establish stressed granulocytes as a promising drug target for developing effective therapy regimens, it is imperative to have more comprehensive data from patients infected with bacterial, viral or fungal infections. In addition, this study mainly focused on PAMP and TLR signaling pathways. Future studies should delineate the role of damage-associated molecular patterns (DAMPs) and other pattern recognition receptors (PRRs), including C-type lectin receptors (CLRs) and RIG-I-like receptors (RLRs) in innate immune memory of stressed granulocytes. Finally, our studies with fractionated granulocytes revealed heterogeneous responses to the secondary stimulus, especially dramatic changes of immune responses and epigenetic reprogramming in mature fraction of granulocytes. Three-dimensional (3D) genome structure and multi-omics studies may enable to better understand the heterogeneity of stressed granulocytes.

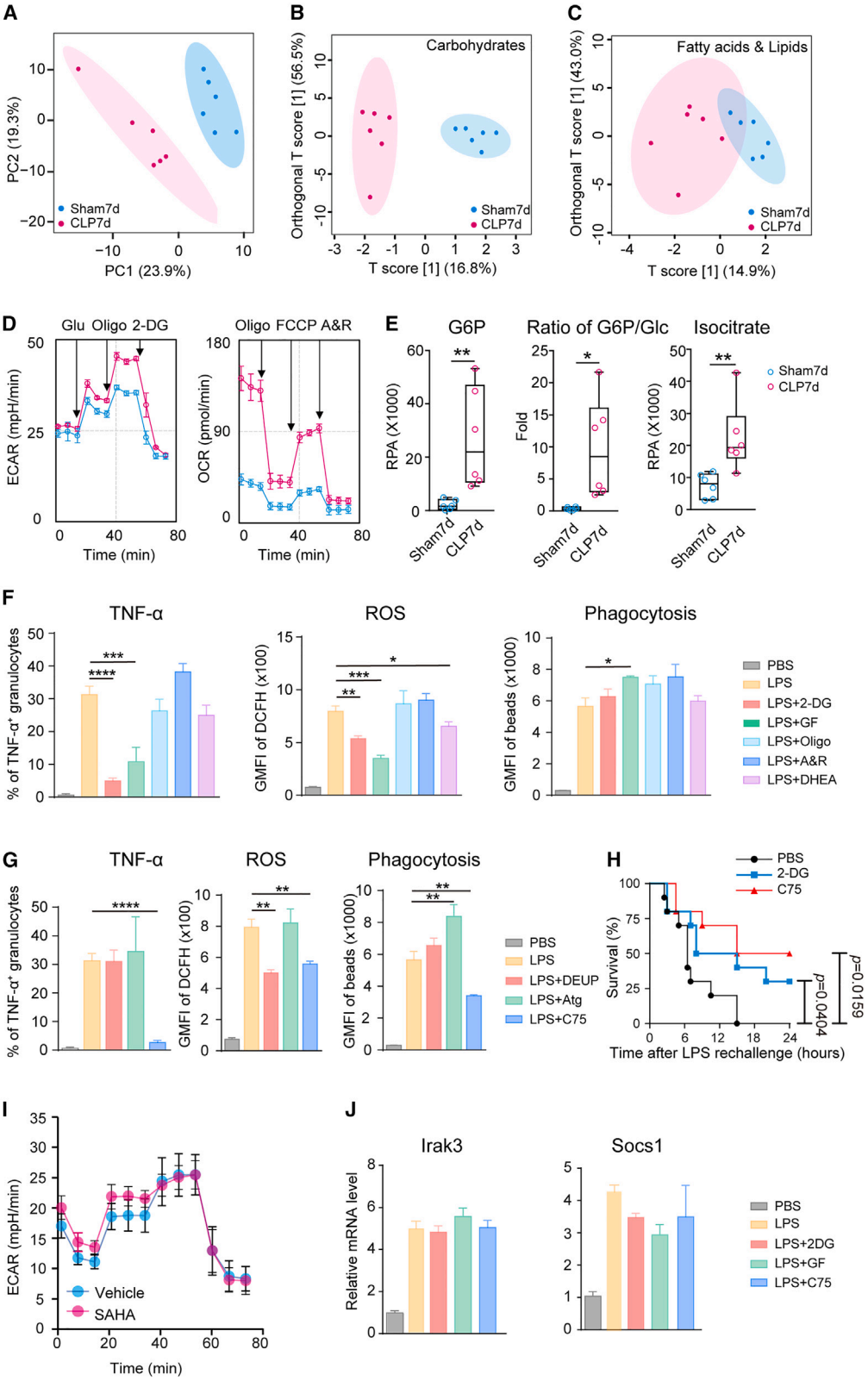

(legend on next page)

STAR★METHODS

Detailed methods are provided in the online version of this paper and include the following:

- KEY RESOURCES TABLE
- RESOURCE AVAILABILITY
  - Lead contact
  - Materials availability
  - Data and code availability
- EXPERIMENTAL MODEL AND STUDY PARTICIPANT DETAILS
- METHOD DETAILS
  - Bacteria strain
  - Sepsis models
  - Secondary infection models
  - Hepatitis models
  - *In vivo* granulocyte depletion
  - Cell preparation
  - Flow cytometry and cell sorting
  - Intracellular staining of TNF-α
  - Multiplex microbead immunoassay for cytokine and chemokine quantification
  - Adoptive cell transfer
  - *In vivo* bioluminescence imaging
  - Histopathology
  - ELISA
  - Cytometric bead array
  - *In vitro* phagocytosis and ROS assays
  - RNA isolation and real-time PCR
  - Western blotting
  - Library preparation of ATAC-seq
  - ATAC-seq data analysis
  - Library preparation for CUT&RUN assays
  - CUT&RUN data analysis
  - Chromatin immunoprecipitation (ChIP)
  - Metabolic flux assay
  - RNA sequencing and bioinformatics analysis
  - ScRNAseq and bioinformatics analysis
- QUANTIFICATION AND STATISTICAL ANALYSIS
  - Statistical analysis

SUPPLEMENTAL INFORMATION

Supplemental information can be found online at https://doi.org/10.1016/j.celrep.2023.113044.

ACKNOWLEDGMENTS

The authors thank Professor Qiang Shan (Institute of Systems Medicine, CAMS) for his assistances in Cut&Run library preparation and Professor Bingxiang Xu (Shanghai University of Sport) for guiding epigenomic data analysis. We also thank Professor Ying Sun (Capital Medical University) and Professor Xiaoning Xu (Imperial College London) for their suggestions and comments during manuscript preparation. This work was supported by grants from the R&D Program of Beijing Municipal Education Commission (KZ202010025041), the National Natural Science Foundation of China General Program (81770069, 81570372, 81871586, 81401624, and 30872458), the Beijing Hospital Authority (DFL20191801), and the high-level public health talents (lingjunrencai-02-06).

AUTHOR CONTRIBUTIONS

H. Zeng and Y.M. designed the study; B.W., L.Z., B.J., C. Zhao, J.Z., J.L., N.D., J.W., and G.L. engaged in the acquisition, analysis, and interpretation of the data; F.L., C. Zhang, Y.H., S.T., H. Zhang, R.L., J.D., Y.K., Y.Z., X.Y., and Y.F. participated in the collection of data; J.H., C.C., and Z.Y. contributed to data analysis and manuscript preparation; Z.D., H. Zheng, A.L., and C.K. contributed to data interpretation; B.W., L.Z., B.J., C. Zhao, and J.Z. drafted the article; and all authors had final approval of the version to be submitted.

DECLARATION OF INTERESTS

The authors declare no competing interests.

Received: January 13, 2023
Revised: July 14, 2023
Accepted: August 14, 2023

REFERENCES

1. Singer, M., Deutschman, C.S., Seymour, C.W., Shankar-Hari, M., Annane, D., Bauer, M., Bellomo, R., Bernard, G.R., Chiche, J.D., Coopersmith, C.M., et al. (2016). The Third International Consensus Definitions for Sepsis and Septic Shock (Sepsis-3). JAMA *315*, 801–810. https://doi.org/10.1001/jama.2016.0287.
2. Fleischmann, C., Scherag, A., Adhikari, N.K.J., Hartog, C.S., Tsaganos, T., Schlattmann, P., Angus, D.C., and Reinhart, K.; International Forum of

Figure 7. Glycolysis and fatty acid synthesis are involved in the innate immunity memory of granulocytes

(A–C) The discrimination of metabolomes in granulocytes from Sham7d (blue dot) and CLP7d mice (red dot) on the basis of gas chromatography/time-of-flight mass spectrometry (GC-TOFMS) analysis. (A) Total metabolites, (B) total carbohydrates, and (C) fatty acids and lipids. For each group, n = 6.

(D) Glycolysis (indicated by the ECAR) and oxidative phosphorylation (indicated by the OCR) were measured under basal conditions and in response to the indicated drugs using a Seahorse XF Analyzer. The blue dot represents granulocytes from Sham7d mice, and the red dot represents granulocytes from CLP7d mice. Glu, glucose; Oligo, oligomycin (an ATP synthase inhibitor); 2-DG, 2-deoxyglucose (a glycolysis inhibitor); FCCP, carbonyl cyanide-p-trifluoromethoxyphenylhydrazone (a protonophore uncoupler); A & R, antimycin A and rotenone (electron transport inhibitors). Data are representative of two independent experiments.

(E) Relative G6P and isocitrate content in the cell extract, as analyzed using GC-TOFMS, and the relative content ratio of G6P versus glucose. n = 6 for each group. RPA, relative peak area.

(F and G) Intracellular staining of TNF-α protein, ROS generation, and phagocytosis in granulocytes from CLP7d mice. GF, galloflavin (a glycolysis inhibitor that specifically inhibits lactic acid dehydrogenase); DHEA, dehydroepiandrosterone (a pentose phosphate pathway inhibitor); DEUP, diethylumbelliferyl phosphate (a pan-lipase inhibitor); Atg, atglistatin (a cytosolic Atgl-lipase inhibitor); C75, a fatty acid synthase inhibitor. Data are representative of two independent experiments (n = 10).

(H) The effects of 2-DG and C75 on the survival rates of CLP7d mice challenged with LPS (10 mg/kg). The drug 2-DG or C75 was intraperitoneally injected into mice synchronously with LPS. For each group, n = 10.

(I) The effect of SAHA on the glycolysis of granulocytes from CLP7d mice. Blue dot, untreated granulocytes; red dot, SAHA pretreatment for 1 h. For each group, n = 6.

(J) The effect of DEUP, Atg, and C75 on mRNA levels of Irak3 and Socs1 in CLP7d granulocytes rechallenged by LPS. For each group, n = 3.

*p < 0.05, **p < 0.01, and ****p < 0.0001 (two-tailed unpaired t test or ANOVA). For each column plot, the bar indicates the mean ± SEM.

Acute Care Trialists (2016). Assessment of Global Incidence and Mortality of Hospital-treated Sepsis. Current Estimates and Limitations. Am. J. Respir. Crit. Care Med. *193*, 259–272. https://doi.org/10.1164/rccm.201504-0781OC.

3. Gotts, J.E., and Matthay, M.A. (2016). Sepsis: pathophysiology and clinical management. BMJ (Clinical research ed.) *353*, i1585. https://doi.org/10.1136/bmj.i1585.
4. Angus, D.C., and Opal, S. (2016). Immunosuppression and Secondary Infection in Sepsis: Part, Not All, of the Story. JAMA *315*, 1457–1459. https://doi.org/10.1001/jama.2016.2762.
5. Faix, J.D. (2013). Biomarkers of sepsis. Crit. Rev. Clin. Lab Sci. *50*, 23–36. https://doi.org/10.3109/10408363.2013.764490.
6. Zhang, J., Liu, J., Yuan, Y., Huang, F., Ma, R., Luo, B., Xi, Z., Pan, T., Liu, B., Zhang, Y., et al. (2020). Two waves of pro-inflammatory factors are released during the influenza A virus (IAV)-driven pulmonary immunopathogenesis. PLoS Pathog. *16*, e1008334. https://doi.org/10.1371/journal.ppat.1008334.
7. van Vught, L.A., Klein Klouwenberg, P.M.C., Spitoni, C., Scicluna, B.P., Wiewel, M.A., Horn, J., Schultz, M.J., Nürnberg, P., Bonten, M.J.M., Cremer, O.L., et al. (2016). Incidence, Risk Factors, and Attributable Mortality of Secondary Infections in the Intensive Care Unit After Admission for Sepsis. JAMA *315*, 1469–1479. https://doi.org/10.1001/jama.2016.2691.
8. Bonilla, F.A., and Oettgen, H.C. (2010). Adaptive immunity. J. Allergy Clin. Immunol. *125*, S33–S40. https://doi.org/10.1016/j.jaci.2009.09.017.
9. Netea, M.G., Domínguez-Andrés, J., Barreiro, L.B., Chavakis, T., Divangahi, M., Fuchs, E., Joosten, L.A.B., van der Meer, J.W.M., Mhlanga, M.M., Mulder, W.J.M., et al. (2020). Defining trained immunity and its role in health and disease. Nat. Rev. Immunol. *20*, 375–388. https://doi.org/10.1038/s41577-020-0285-6.
10. Netea, M.G., Joosten, L.A.B., Latz, E., Mills, K.H.G., Natoli, G., Stunnenberg, H.G., O'Neill, L.A.J., and Xavier, R.J. (2016). Trained immunity: A program of innate immune memory in health and disease. Science *352*, aaf1098. https://doi.org/10.1126/science.aaf1098.
11. Netea, M.G., Schlitzer, A., Placek, K., Joosten, L.A.B., and Schultze, J.L. (2019). Innate and Adaptive Immune Memory: an Evolutionary Continuum in the Host's Response to Pathogens. Cell Host Microbe *25*, 13–26. https://doi.org/10.1016/j.chom.2018.12.006.
12. de Laval, B., Maurizio, J., Kandalla, P.K., Brisou, G., Simonnet, L., Huber, C., Gimenez, G., Matcovitch-Natan, O., Reinhardt, S., David, E., et al. (2020). C/EBPβ-Dependent Epigenetic Memory Induces Trained Immunity in Hematopoietic Stem Cells. Cell Stem Cell *26*, 657–674.e8. https://doi.org/10.1016/j.stem.2020.01.017.
13. Schlums, H., Cichocki, F., Tesi, B., Theorell, J., Beziat, V., Holmes, T.D., Han, H., Chiang, S.C.C., Foley, B., Mattsson, K., et al. (2015). Cytomegalovirus infection drives adaptive epigenetic diversification of NK cells with altered signaling and effector function. Immunity *42*, 443–456. https://doi.org/10.1016/j.immuni.2015.02.008.
14. Song, W.M., and Colonna, M. (2018). Immune Training Unlocks Innate Potential. Cell *172*, 3–5. https://doi.org/10.1016/j.cell.2017.12.034.
15. Yoshida, K., Maekawa, T., Zhu, Y., Renard-Guillet, C., Chatton, B., Inoue, K., Uchiyama, T., Ishibashi, K.-i., Yamada, T., Ohno, N., et al. (2015). The transcription factor ATF7 mediates lipopolysaccharide-induced epigenetic changes in macrophages involved in innate immunological memory. Nat. Immunol. *16*, 1034–1043. https://doi.org/10.1038/ni.3257.
16. Divangahi, M., Aaby, P., Khader, S.A., Barreiro, L.B., Bekkering, S., Chavakis, T., van Crevel, R., Curtis, N., DiNardo, A.R., Dominguez-Andres, J., et al. (2021). Trained immunity, tolerance, priming and differentiation: distinct immunological processes. Nat. Immunol. *22*, 2–6. https://doi.org/10.1038/s41590-020-00845-6.
17. Fanucchi, S., Domínguez-Andrés, J., Joosten, L.A.B., Netea, M.G., and Mhlanga, M.M. (2021). The Intersection of Epigenetics and Metabolism in Trained Immunity. Immunity *54*, 32–43. https://doi.org/10.1016/j.immuni.2020.10.011.
18. Arts, R.J.W., Moorlag, S.J.C.F.M., Novakovic, B., Li, Y., Wang, S.-Y., Oosting, M., Kumar, V., Xavier, R.J., Wijmenga, C., Joosten, L.A.B., et al. (2018). BCG Vaccination Protects against Experimental Viral Infection in Humans through the Induction of Cytokines Associated with Trained Immunity. Cell Host Microbe *23*, 89–100.e5. https://doi.org/10.1016/j.chom.2017.12.010.
19. Ter Steeg, L., Domínguez-Andrés, J., Netea, M.G., Joosten, L.A.B., and van Crevel, R. (2021). Trained Immunity as a Preventive Measure for Surgical Site Infections. Clin. Microbiol. Rev. *34*, e0004921. https://doi.org/10.1128/CMR.00049-21.
20. Saeed, S., Quintin, J., Kerstens, H.H.D., Rao, N.A., Aghajanirefah, A., Matarese, F., Cheng, S.C., Ratter, J., Berentsen, K., van der Ent, M.A., et al. (2014). Epigenetic programming of monocyte-to-macrophage differentiation and trained innate immunity. Science *345*, 1251086. https://doi.org/10.1126/science.1251086.
21. Kalafati, L., Kourtzelis, I., Schulte-Schrepping, J., Li, X., Hatzioannou, A., Grinenko, T., Hagag, E., Sinha, A., Has, C., Dietz, S., et al. (2020). Innate Immune Training of Granulopoiesis Promotes Anti-tumor Activity. Cell *183*, 771–785.e12. https://doi.org/10.1016/j.cell.2020.09.058.
22. Arts, R.J.W., Novakovic, B., Ter Horst, R., Carvalho, A., Bekkering, S., Lachmandas, E., Rodrigues, F., Silvestre, R., Cheng, S.C., Wang, S.-Y., et al. (2016). Glutaminolysis and Fumarate Accumulation Integrate Immunometabolic and Epigenetic Programs in Trained Immunity. Cell Metabol. *24*, 807–819. https://doi.org/10.1016/j.cmet.2016.10.008.
23. Bekkering, S., Arts, R.J.W., Novakovic, B., Kourtzelis, I., van der Heijden, C.D.C.C., Li, Y., Popa, C.D., Ter Horst, R., van Tuijl, J., Netea-Maier, R.T., et al. (2018). Metabolic Induction of Trained Immunity through the Mevalonate Pathway. Cell *172*, 135–146.e9. https://doi.org/10.1016/j.cell.2017.11.025.
24. Kaufmann, E., Sanz, J., Dunn, J.L., Khan, N., Mendonça, L.E., Pacis, A., Tzelepis, F., Pernet, E., Dumaine, A., Grenier, J.C., et al. (2018). BCG Educates Hematopoietic Stem Cells to Generate Protective Innate Immunity against. Tuberculosis. Cell *172*, 176–190.e19. https://doi.org/10.1016/j.cell.2017.12.031.
25. Xu, L., Zhang, W., Kwak, M., Zhang, L., Lee, P.C.W., and Jin, J.-O. (2019). Protective Effect of Melatonin Against Polymicrobial Sepsis Is Mediated by the Anti-bacterial Effect of Neutrophils. Front. Immunol. *10*, 1371. https://doi.org/10.3389/fimmu.2019.01371.
26. Yo, C.H., Hsein, Y.C., Wu, Y.L., Hsu, W.T., Ma, M.H.M., Tsai, C.H., Chen, S.C., and Lee, C.C. (2019). Clinical predictors and outcome impact of community-onset polymicrobial bloodstream infection. Int. J. Antimicrob. Agents *54*, 716–722. https://doi.org/10.1016/j.ijantimicag.2019.09.015.
27. King, K.Y., and Goodell, M.A. (2011). Inflammatory modulation of HSCs: viewing the HSC as a foundation for the immune response. Nat. Rev. Immunol. *11*, 685–692. https://doi.org/10.1038/nri3062.
28. Chen, Y., Hu, Y., Zhang, J., Shen, Y., Huang, J., Yin, J., Wang, P., Fan, Y., Wang, J., Lu, S., et al. (2019). Clinical characteristics, risk factors, immune status and prognosis of secondary infection of sepsis: a retrospective observational study. BMC Anesthesiol. *19*, 185. https://doi.org/10.1186/s12871-019-0849-9.
29. Kwok, I., Becht, E., Xia, Y., Ng, M., Teh, Y.C., Tan, L., Evrard, M., Li, J.L.Y., Tran, H.T.N., Tan, Y., et al. (2020). Combinatorial Single-Cell Analyses of Granulocyte-Monocyte Progenitor Heterogeneity Reveals an Early Uni-potent Neutrophil Progenitor. Immunity *53*, 303–318.e5. https://doi.org/10.1016/j.immuni.2020.06.005.
30. Gereke, M., Gröbe, L., Prettin, S., Kasper, M., Deppenmeier, S., Gruber, A.D., Enelow, R.I., Buer, J., and Bruder, D. (2007). Phenotypic alterations in type II alveolar epithelial cells in CD4+ T cell mediated lung inflammation. Respir. Res. *8*, 47. https://doi.org/10.1186/1465-9921-8-47.
31. Lentini, G., Famà, A., Biondo, C., Mohammadi, N., Galbo, R., Mancuso, G., Iannello, D., Zummo, S., Giardina, M., De Gaetano, G.V., et al. (2020). Neutrophils Enhance Their Own Influx to Sites of Bacterial Infection via Endosomal TLR-Dependent Cxcl2 Production. J. Immunol. *204*, 660–670. https://doi.org/10.4049/jimmunol.1901039.

32. Rydström, A., and Wick, M.J. (2009). Monocyte and neutrophil recruitment during oral Salmonella infection is driven by MyD88-derived chemokines. Eur. J. Immunol. *39*, 3019–3030. https://doi.org/10.1002/eji.200939483.

33. Nauseef, W.M., and Borregaard, N. (2014). Neutrophils at work. Nat. Immunol. *15*, 602–611. https://doi.org/10.1038/ni.2921.

34. Jia, B., Zhao, C., Li, G., Kong, Y., Ma, Y., Wang, Q., Wang, B., and Zeng, H. (2017). A Novel CD48-Based Analysis of Sepsis-Induced Mouse Myeloid-Derived Suppressor Cell Compartments. Mediat. Inflamm. *2017*, 7521701. https://doi.org/10.1155/2017/7521701.

35. Cassatella, M.A., Östberg, N.K., Tamassia, N., and Soehnlein, O. (2019). Biological Roles of Neutrophil-Derived Granule Proteins and Cytokines. Trends Immunol. *40*, 648–664. https://doi.org/10.1016/j.it.2019.05.003.

36. Dennis, G., Jr., Sherman, B.T., Hosack, D.A., Yang, J., Gao, W., Lane, H.C., and Lempicki, R.A. (2003). DAVID: Database for Annotation, Visualization, and Integrated Discovery. Genome Biol. *4*, P3.

37. Subramanian, A., Tamayo, P., Mootha, V.K., Mukherjee, S., Ebert, B.L., Gillette, M.A., Paulovich, A., Pomeroy, S.L., Golub, T.R., Lander, E.S., and Mesirov, J.P. (2005). Gene set enrichment analysis: a knowledge-based approach for interpreting genome-wide expression profiles. Proc. Natl. Acad. Sci. USA *102*, 15545–15550. https://doi.org/10.1073/pnas.0506580102.

38. Shan, Q., Zhu, S., Chen, X., Liu, J., Yuan, S., Li, X., Peng, W., and Xue, H.H. (2022). Tcf1-CTCF cooperativity shapes genomic architecture to promote CD8(+) T cell homeostasis. Nat. Immunol. *23*, 1222–1235. https://doi.org/10.1038/s41590-022-01263-6.

39. Jentho, E., Ruiz-Moreno, C., Novakovic, B., Kourtzelis, I., Megchelenbrink, W.L., Martins, R., Chavakis, T., Soares, M.P., Kalafati, L., Guerra, J., et al. (2021). Trained innate immunity, long-lasting epigenetic modulation, and skewed myelopoiesis by heme. Proc. Natl. Acad. Sci. USA *118*, e2102698118. https://doi.org/10.1073/pnas.2102698118.

40. Kleinnijenhuis, J., Quintin, J., Preijers, F., Joosten, L.A.B., Ifrim, D.C., Saeed, S., Jacobs, C., van Loenhout, J., de Jong, D., Stunnenberg, H.G., et al. (2012). Bacille Calmette-Guerin induces NOD2-dependent nonspecific protection from reinfection via epigenetic reprogramming of monocytes. Proc. Natl. Acad. Sci. USA *109*, 17537–17542. https://doi.org/10.1073/pnas.1202870109.

41. Wimmers, F., Donato, M., Kuo, A., Ashuach, T., Gupta, S., Li, C., Dvorak, M., Foecke, M.H., Chang, S.E., Hagan, T., et al. (2021). The single-cell epigenomic and transcriptional landscape of immunity to influenza vaccination. Cell *184*, 3915–3935.e21. https://doi.org/10.1016/j.cell.2021.05.039.

42. You, M., Chen, L., Zhang, D., Zhao, P., Chen, Z., Qin, E.Q., Gao, Y., Davis, M.M., and Yang, P. (2021). Single-cell epigenomic landscape of peripheral immune cells reveals establishment of trained immunity in individuals convalescing from COVID-19. Nat. Cell Biol. *23*, 620–630. https://doi.org/10.1038/s41556-021-00690-1.

43. Bird, L. (2020). Trained immunity by HSCs. Nat. Rev. Immunol. *20*, 276–277. https://doi.org/10.1038/s41577-020-0299-0.

44. Gabrilovich, D.I., and Nagaraj, S. (2009). Myeloid-derived suppressor cells as regulators of the immune system. Nat. Rev. Immunol. *9*, 162–174. https://doi.org/10.1038/nri2506.

45. Talmadge, J.E., and Gabrilovich, D.I. (2013). History of myeloid-derived suppressor cells. Nat. Rev. Cancer *13*, 739–752. https://doi.org/10.1038/nrc3581.

46. Novotny, A.R., Reim, D., Assfalg, V., Altmayr, F., Friess, H.M., Emmanuel, K., and Holzmann, B. (2012). Mixed antagonist response and sepsis severity-dependent dysbalance of pro- and anti-inflammatory responses at the onset of postoperative sepsis. Immunobiology *217*, 616–621. https://doi.org/10.1016/j.imbio.2011.10.019.

47. Zhao, G.J., Li, D., Zhao, Q., Song, J.X., Chen, X.R., Hong, G.L., Li, M.F., Wu, B., and Lu, Z.Q. (2016). Incidence, risk factors and impact on outcomes of secondary infection in patients with septic shock: an 8-year retrospective study. Sci. Rep. *6*, 38361. https://doi.org/10.1038/srep38361.

48. Hubbard, W.J., Choudhry, M., Schwacha, M.G., Kerby, J.D., Rue, L.W., 3rd, Bland, K.I., and Chaudry, I.H. (2005). Cecal ligation and puncture. Shock *24* (*Suppl 1*), 52–57. https://doi.org/10.1097/01.shk.0000191414.94461.7e.

49. Pertea, M., Kim, D., Pertea, G.M., Leek, J.T., and Salzberg, S.L. (2016). Transcript-level expression analysis of RNA-seq experiments with HISAT, StringTie and Ballgown. Nat. Protoc. *11*, 1650–1667. https://doi.org/10.1038/nprot.2016.095.

50. Kim, D., Langmead, B., and Salzberg, S.L. (2015). HISAT: a fast spliced aligner with low memory requirements. Nat. Methods *12*, 357–360. https://doi.org/10.1038/nmeth.3317.

51. Pertea, M., Pertea, G.M., Antonescu, C.M., Chang, T.C., Mendell, J.T., and Salzberg, S.L. (2015). StringTie enables improved reconstruction of a transcriptome from RNA-seq reads. Nat. Biotechnol. *33*, 290–295. https://doi.org/10.1038/nbt.3122.

52. Frazee, A.C., Pertea, G., Jaffe, A.E., Langmead, B., Salzberg, S.L., and Leek, J.T. (2015). Ballgown bridges the gap between transcriptome assembly and expression analysis. Nat. Biotechnol. *33*, 243–246. https://doi.org/10.1038/nbt.3172.

53. Sherman, B.T., Hao, M., Qiu, J., Jiao, X., Baseler, M.W., Lane, H.C., Imamichi, T., and Chang, W. (2022). DAVID: a web server for functional enrichment analysis and functional annotation of gene lists (2021 update). Nucleic Acids Res. *50*, W216–W221. https://doi.org/10.1093/nar/gkac194.

54. Yu, G., Wang, L.G., Han, Y., and He, Q.Y. (2012). clusterProfiler: an R package for comparing biological themes among gene clusters. OMICS A J. Integr. Biol. *16*, 284–287. https://doi.org/10.1089/omi.2011.0118.

55. Butler, A., Hoffman, P., Smibert, P., Papalexi, E., and Satija, R. (2018). Integrating single-cell transcriptomic data across different conditions, technologies, and species. Nat. Biotechnol. *36*, 411–420. https://doi.org/10.1038/nbt.4096.

56. Satija, R., Farrell, J.A., Gennert, D., Schier, A.F., and Regev, A. (2015). Spatial reconstruction of single-cell gene expression data. Nat. Biotechnol. *33*, 495–502. https://doi.org/10.1038/nbt.3192.

57. Trapnell, C., Cacchiarelli, D., Grimsby, J., Pokharel, P., Li, S., Morse, M., Lennon, N.J., Livak, K.J., Mikkelsen, T.S., and Rinn, J.L. (2014). The dynamics and regulators of cell fate decisions are revealed by pseudotemporal ordering of single cells. Nat. Biotechnol. *32*, 381–386. https://doi.org/10.1038/nbt.2859.

58. Dobin, A., Davis, C.A., Schlesinger, F., Drenkow, J., Zaleski, C., Jha, S., Batut, P., Chaisson, M., and Gingeras, T.R. (2013). STAR: ultrafast universal RNA-seq aligner. Bioinformatics *29*, 15–21. https://doi.org/10.1093/bioinformatics/bts635.

STAR★METHODS

KEY RESOURCES TABLE

REAGENT or RESOURCE	SOURCE	IDENTIFIER
Antibodies		
anti-mouse CD11b (clone M1/70)	BD	Cat#550993; RRID: AB_394002
anti-mouse Ly6G (clone 1A8)	BD	Cat#740157; RRID: AB_2739910
anti-mouse CD48 (clone HM48-1)	Biolegend	Cat#103412; RRID: AB_571996
anti-mouse Gr-1 (clone RB6-8C5)	BD	Cat#553127; RRID: AB_394643
anti-mouse TNF-α (cloneMP6-XT22)	BD	Cat#554419; RRID: AB_395380
anti-TNF-α	Cell Signaling Technology	Cat#3707; RRID:AB_2240625
anti-IRAK-M	Abcam	Catalog #ab8116; RRID:AB_306286
anti-SHP-1	Cell Signaling Technology	Catalog #26516; RRID:AB_2934293
anti-SOCS-1	Cell Signaling Technology	Catalog #55313
anti-β-actin	Cell Signaling Technology	Catalog #3700; RRID:AB_2242334
anti-H3K27Ac	Abcam	Catalog #ab4729; RRID:AB_2118291
anti-H3K9ac	Abcam	Catalog #ab32129; RRID:AB_732920
anti-H3K4me2	Abcam	Catalog #ab32356; RRID:AB_732924
Bacterial and virus strains		
Pseudomonas aeruginosa	The Institute of Burn Research South-West Hospital, Chongqing, China	ATCC15692
Chemicals, peptides, and recombinant proteins		
E.coli derived ultrapure LPS (serotype0111:B4)	Sigma-Aldrich	Cat#L-2630
Trizol	Invitrogen	Cat#15596018
CD11b magnetic MicroBeads	Miltenyi	Cat#130-126-725
COUNTING BEADS	BD	Cat#340334
GolgiPlug™ Protein Transport Inhibitor (Containing Brefeldin A)	BD	Cat# 555029
BD Cytofix/Cytoperm™ Fixation/ Permeabilization Kit	BD	Cat# 554714
ProcartaPlex mouse Cytokine & Chemokine 36-plex kit	Thermo Fisher Scientific	Cat#EPX360-26092-901
Mouse TNF ELISA Kit	BD	Cat#560478
Yellow-green latex beads	Thermo Fisher Scientific	Cat#L4655
2′,7′-dichlorofluorescin diacetate	Sigma-Aldrich	Cat#D6883
phorbol myristate acetate	Sigma-Aldrich	Cat#P8139
C75	Sigma-Aldrich	Cat#C5490
2-DG	Sigma-Aldrich	Cat#D8375
SB225002	Selleck	Cat#S7651
Clodronate Liposomes	LIPOSOMA	Cat#CP-005-005
anti-Ly6G monoclonal antibody (clone 1A8)	InVivoMab BioXCell	Cat#BE0075-1; RRID:AB_10312146
Isotype control Ig	InVivoMab BioXCell	Cat#BE0089; RRID:AB_1107769
Etanercept (soluble recombinant TNF receptor II)	Shanghai CP Guojian Pharmaceutical Co., Shanghai, China	N/A
SAHA	Selleck	Cat#S1047
con A	Sigma-Aldrich	Cat#C2010
Cytometric bead array (Mouse Inflammation Kit)	BD	Cat#552364
poly-L-lysine	Sigma-Aldrich	Cat#P4832

(*Continued on next page*)

Continued

REAGENT or RESOURCE	SOURCE	IDENTIFIER
antimycin A/Rotenone, A&R	abcam	Cat#ab52922
Oligomycin	MedChemExpres	Cat#HY-N6782
DHEA	MedChemExpress	Cat#HY-14650
DEUP	Sigma-Aldrich	Cat#D7692
Atglistatin	Sigma-Aldrich	Cat#SML1075
Galloflavin	Sigma-Aldrich	Cat#PHL83342
concanavalin A	Sigma-Aldrich	Catalog #C2010
Percoll gradient	GE Healthcare	Catalog #17-0891-02
RPMI 1640 medium	Gibco	Catalog #A1049101
High-Capacity cDNA Reverse Transcription Kit	Applied Biosystems	Catalog # 4374966
protease inhibitor cocktail	Sigma-Aldrich	Catalog #539131
Protein A/G Dynabeads	Thermo Fisher Scientific	Catalog # 80104G
NEBNext Ultra Directional RNA Library Prep Kit	NEB	Catalog #E7760
TruSeq PE Cluster Kit v3-cBot-HS	Illumina	Catalog # PE-401-3001
Deposited data		
RNA-seq data	National Genomics Data Center	accession number CRA001737
scRNA-seq data	National Genomics Data Center	accession number CRA001040
ATAC-seq data	NCBI SRA	PRJNA994272
CUT&RUN data	NCBI SRA	PRJNA994272
Original Code	This paper	https://ngdc.cncb.ac.cn/biocode/tools/BT007379; https://github.com/IID-DTH/RscriptsForGranulocytesDynamics
Experimental models: Organisms/strains		
C57BL/6J Mice	The Institute of Laboratory Animal Science, Chinese Academy of Medical Science	N/A
Luciferase-expressing mice	Gift from Prof. Zhang Wei, Peking University Hepatology Institute	N/A
Oligonucleotides		
ChIP primer Irak3-F	5′-CGTTCCTGCGGTGGTCATTACA-3′	N/A
ChIP primer Irak3-R	5′-AGGCCAAACCTGGGCAAACAAA-3′	N/A
ChIP primer Ptpn6-F	5′-AGGGCTGGCAAGCAGAATTCAA-3′	N/A
ChIP primer Ptpn6-R	5′-TCACCAGGGCCTCATTCCTCAG-3′	N/A
ChIP primer Socs1-F	5′-GTTCCAAGAAGGGTCGAGATTGC-3′	N/A
ChIP primer Socs1-R	5′-GCCCGCTCTTTTGCTCTACCT-3′	N/A
Software and algorithms		
FlowJo software v10.1	TreeStar	https://www.flowjo.com/
GraphPad Prism7	GraphPad Software	https://www.graphpad.com/
Bowtie2	Johns Hopkins University	https://bowtie-bio.sourceforge.net/bowtie2/index.shtml
fastQC	Babraham Institute	https://www.bioinformatics.babraham.ac.uk/projects/fastqc/
fastp	HaploX Biotechnology	https://github.com/OpenGene/fastp
Trimmomatic	RWTH Aachen University. Usadel's lab	https://github.com/usadellab/Trimmomatic
Picard	Broad Institute	http://broadinstitute.github.io/picard
MACS3	Harvard University, Xiaole S. Liu's Lab	https://github.com/taoliu/MACS
SEACR	Howard Hughes Medical Institute	https://github.com/FredHutch/SEACR
samtools	Sanger Institute and Broad Institute	https://www.htslib.org/
bedtools	University of Utah, Quinlan Lab	http://bedtools.readthedocs.io/en/latest/

(*Continued on next page*)

Continued

REAGENT or RESOURCE	SOURCE	IDENTIFIER
deeptools	Max Planck Institute for Immunobiology and Epigenetics	https://deeptools.readthedocs.io/en/latest/index.html
DiffBind	Bioconductor	https://bioconductor.org/packages/release/bioc/html/DiffBind.html
ChIPSeeker	Bioconductor	https://bioconductor.org/packages/release/bioc/html/ChIPseeker.html
clusterProfiler	Bioconductor	https://bioconductor.org/packages/release/bioc/html/clusterProfiler.html
IGV	UC San Diego, the Broad Institute of MIT and Harvard	https://igv.org/

RESOURCE AVAILABILITY

Lead contact

Further information and requests for resources and reagents should be directed to and will be fulfilled by the lead contact, Hui Zeng (zenghui@ccmu.edu.cn).

Materials availability

This study did not generate new unique reagents.

Data and code availability

- All sequencing data and original code have been deposited at public database and are publicly available as of the date of publication. Accession numbers are listed in the key resources table.
- Any additional information required to reanalyze the data reported in this paper is available from the lead contact upon request.

EXPERIMENTAL MODEL AND STUDY PARTICIPANT DETAILS

Wild-type male C57BL/6J and BALB/c mice (6–8 weeks old) were purchased from the Institute of Laboratory Animal Science, Chinese Academy of Medical Science (Beijing, China). Littermates were housed in a specific-pathogen-free facility and had access to distilled water *ad libitum*. All animal procedures were carried out in compliance with the Animal Care Research Ethics Committee of the Capital Medical University, Beijing, China (sjtkl11-1x-2022(060)).

All the experiments were repeated at least three times independently.

METHOD DETAILS

Bacteria strain

P. aeruginosa (strain PAO.1 was kindly provided by the Institute of Burn Research South-West Hospital, Chongqing, China) were expanded in Luria-Bertani (LB) broth. Before inoculation, *P. aeruginosa* were cultured overnight in LB broth at 37°C with constant shaking and harvested in PBS. The infectious dose was determined by plating on LB-agar plates with 10-fold serial dilutions.

Sepsis models

All procedures performed on animals were approved by the Animal Care Research Ethics Committee of the Capital Medical University of China. An animal model of sepsis was established by the CLP procedure, as previously described.[48] Briefly, C57BL/6J or luciferase-expressing mice were anesthetized by the i.p. injection of ketamine (100 mg/kg body weight) and xylazine (0.1 mL/10 g body weight). Midline laparotomy was performed after skin was disinfected with iodine tincture (2%). The cecum was exposed and ligated at half the distance between the distal pole and the base of the cecum with a 3-0 silk suture followed by puncture with an 18-gauge needle. Tissue layers of the abdominal wall and skin were closed with 4-0 polypropylene sutures. Sterile saline (1 mL) was subcutaneously injected for fluid resuscitation during the postoperative period. Mice were monitored over the next 7 days before subsequent experiments. The survival rate of the CLP model was about 50%, and the status of the survival CLP7d mice was already recovered. The surviving mice were then randomly grouped for the secondary stimulus.

Secondary infection models

To induce an acute inflammatory response, CLP mice 7 days postsurgery (CLP7d mice) were intraperitoneally injected with *Escherichia coli* LPS (Sigma-Aldrich, St. Louis, MO) at a single dose of 10 mg/kg body weight. For gradual bacterial infection, CLP7d mice were intratracheally infected with *P. aeruginosa* (2×10^9 CFU in 50 μL of PBS).

Two methods were used to rescue septic mice from secondary infections: 1) CLP7d mice were intraperitoneally administered 12.5 mg/kg soluble recombinant TNF receptor II (Shanghai CP Guojian Pharmaceutical Co., Shanghai, China) 18 h before and 1 h after LPS injection or *P. aeruginosa* inoculation. 2) CLP7d mice were intraperitoneally administered 50 mg/kg SAHA (Selleck Chemicals, Houston, TX) 1 h prior to or at the same time as LPS challenge. All mice were monitored to evaluate the survival rate or were euthanized for tissue harvesting at individual time points.

Hepatitis models

Two liver injury models were used for the adoptive-transfer experiment. For the autoimmune hepatitis model, con A (Sigma-Aldrich, St. Louis, MO, USA) was dissolved in sterile PBS and injected through the retro-orbital plexus at a dose of 12.5 mg/kg per C57BL/6J mouse.

In vivo granulocyte depletion

To deplete granulocytes *in vivo*, mice were intraperitoneally injected with 500 μg/kg anti-Ly6G monoclonal antibody (mAb) (InVivoMab clone 1A8, BioXCell, West Lebanon, NH) or 500 μg/kg isotype control Ig (InVivoMab clone 2A3, BioXCell). The efficiency of granulocyte depletion was verified by flow cytometry.

Cell preparation

Mice were sacrificed after being anesthetized. Peripheral blood was collected into spray-coated K_2EDTA tubes (BD Vacutainer, Franklin Lakes, NJ, USA) via retrobulbar vein puncture. Bone marrow cells were flushed from the femurs and tibias with PBS (Gibco, Thermo Fisher Scientific, Waltham, MA, USA) supplemented with 0.5% w/v bovine serum albumin (BSA) and 2 mM EDTA (staining buffer) after bilateral hindlimb dissection. The spleen, lung and liver were surgically removed and homogenized with a 70-μm cell strainer (BD Falcon, Bedford, MA, USA) under aseptic conditions. To separate leukocytes from hepatocytes of the liver, leukocytes were collected at the interface between a 40% and 80% discontinuous Percoll gradient (GE Healthcare, Pittsburgh, PA, USA) as previously described and rinsed with staining buffer. Isolated cells were resuspended in either RPMI 1640 medium supplemented with 10% FBS and 1% penicillin and streptomycin (R10 medium) for *ex vivo* culture, staining buffer for flow cytometry staining, or PBS for cell morphology assays, adoptive transfer, cell metabolic assays and RNA/DNA/protein extraction.

Flow cytometry and cell sorting

Cells were labeled with the following fluorochrome-labeled mAbs: anti-CD45-FITC (BD Bioscience, San Jose, CA, USA), anti-CD48-APC (Biolegend, San Diego, CA, USA), anti-CD11b-PerCP/Cy5.5 (BD Bioscience, San Jose, CA, USA), and anti-Gr1-PE (BD Bioscience, San Jose, CA, USA). Isotype control antibodies were used in each staining procedure. For surface marker labeling, single cell suspensions were stained with mixed fluorochrome-labeled mAbs in staining buffer for 20 min in the dark at 4°C. To quantify the absolute cell number, flow cytometry cell counting beads (BD Bioscience, San Jose, CA, USA) were diluted and added to samples before data acquisition. Cells were analyzed on a BD LSR Fortessa or BD FACSCalibur (BD Biosciences, Franklin Lakes, NJ, USA) according to the manufacturer's instructions. All data were analyzed with FlowJo software (version 10.1; Tree Star, Ashland, OR).

For cell sorting, bone marrow cells were stained with anti-CD11b-PerCP/Cy5.5, anti-CD48-APC, and anti-Gr1-PE and sorted with a BD FACS Aria II flow cytometer (BD Biosciences, Franklin Lakes, NJ, USA) to purify granulocytes and monocytes.

Intracellular staining of TNF-α

For TNF-α intracellular staining, cells from the bone marrow, spleen and lung were cultured in the presence of 10 μg/mL Golgi Plug (brefeldin A, BD Bioscience, San Jose, CA, USA) with or without LPS (100 ng/mL) stimulation for 3 h. Stimulated cells were first stained with cell surface marker antibodies (anti-CD11b-PerCP/Cy5.5, anti-Gr1FITC and anti-CD48-APC) and then were fixed and permeabilized using a Fixation/Permeabilization Kit (BD Bioscience, San Jose, CA) for 20 min. Cells were then washed in Perm/Wash buffer and stained with anti-TNF-α-PE (BD Bioscience) for 30 min at 4°C. The stained cells were then assayed by flow cytometry.

Multiplex microbead immunoassay for cytokine and chemokine quantification

The cytokine and chemokine levels in mice sera were measured using ProcartaPlex mouse Cytokine & Chemokine 36-plex kit (Thermo Fisher Scientific) according to the operating instruction. Data were acquired on a Luminex FlexMap 200 instrument (Millipore) and analyzed using Bio-plex Manager6.0 software (Bio-Rad Laboratories) based on standard curves plotted through a five-parameter logistic curve setting.

The cytokines and chemokines assays included IFN-γ, IL-12p70, IL-13, IL1β, IL-2, IL-4, IL-5, IL-6, TNFα, GM-CSF, IL-18, IL-10, IL-17A, IL-22, IL-23, IL-27, IL-9, GRO α, IP-10, MCP-1, MCP-3, MIP-1 α, MIP-1 β, MIP-2, RANTES, Eotaxin, IFN-α, IL-15/IL-15R, IL-28, IL-31, IL-1α, IL-3, G-CSF, LIF, ENA-78/CXCL5, and M-CSF.

The concentrations were then logarithmically transformed before further analysis to ensure normality. Two-way ANOVAs were used to detect analytes that differ between sample groups over time.

Adoptive cell transfer

Granulocytes from CLP7d mice were purified by fluorescence-activated cell sorting and washed with sterile PBS. Naive mice were intravenously injected with 5×10^6 granulocytes (100 μL per mouse) 1 h prior to Con A injection. Control mice received 100 μL sterile PBS instead of granulocytes during the same procedure. All mice were monitored for 24 h for survival observations or plasma was collected for ALT and AST tests 12 h after Con A injection.

In vivo bioluminescence imaging

In vivo quantitative fluorescence and bioluminescence imaging were performed with an *In Vivo* Imaging System (IVIS) Lumina II Imaging System (Caliper Life Sciences, Hopkinton, Massachusetts, United States). The signals were normalized and monitored by Living Image 4.0 software. Donor granulocytes from Sham7d or CLP7d luc mice were collected from the bone marrow and purified by fluorescence-activated cell sorting, as previously described. LPS (10 mg/kg) or PBS (control) was intraperitonially injected into Sham7d or CLP7d recipient mice. One hour later, 5×10^6 granulocytes from donor mice were slowly injected into the tail vein of recipient mice. All recipient mice were anesthetized with isoflurane (Abbott Laboratories, Shanghai, China) and placed in the IVIS imaging system for analysis (n = 4 for each group). Optimal times of exposure were determined, and images were taken by Living Image 4.0 software according to the manufacturer's instructions.

Histopathology

Lungs and livers from CLP7d mice challenged with LPS or PBS were fixed with 10% neutral buffered formalin for at least 72 h, embedded in paraffin, and sectioned. Tissues were stained with hematoxylin and eosin (H&E) for histopathological examination. All representative images were taken under a microscope (Olympus Corporation, Shinjuku, Tokyo, Japan) with cellSens software (Olympus Corporation).

ELISA

Granulocytes in the bone marrow of CLP7d mice were purified as previously described and cultured in RPMI 1640 medium in the presence of 10% FBS and LPS (100 ng/mL) for the intended period. Supernatants from each time point were collected for TNF-α measurements using a commercial ELISA kit (BD Bioscience) following the manufacturer's instructions.

Cytometric bead array

Inflammatory cytokines, including TNF-α, IL-6, MCP-1, IFN-γ, IL-12 and IL-10, in plasma were quantified by using a Cytometric bead array (Mouse Inflammation Kit, BD Bioscience). Samples were processed with a BD FACSCalibur and analyzed with Cell Quest software (BD Bioscience) according to the manufacturer's instructions.

In vitro phagocytosis and ROS assays

Cells from the bone marrow and spleen of CLP7d mice and Sham7d mice were harvested, as described above. $CD11b^+$ cells were purified using anti-CD11b magnetic beads (Miltenyi Biotec, Germany). For the phagocytosis assay, 5×10^5 cells were seeded in 96-well plates and stimulated with LPS (100 ng/mL). Yellow-green latex beads (Thermo Fisher Scientific, Waltham, MA) were then added to the media to allow engulfment. After a 4-h incubation at 37°C, cells were further stained with anti-CD11b-PerCP, anti-CD48-APC and anti-Gr1-PE to analyze surface markers. A short incubation (1 min) with trypan blue was used to quench bead binding at the cell surface before flow cytometry analysis (BD FACSCalibur). To measure cellular ROS, 5×10^5 cells in culture media were stained with 2′,7′-dichlorofluorescin diacetate (DCFH-DA, 0.01 μg/mL, Sigma-Aldrich) and stimulated with phorbol myristate acetate (PMA, 0.1 μg/mL, Sigma-Aldrich) for 7 min at 37°C. Cells stimulated with PMA only were used as controls. After incubation, cells were stained with surface markers as described above and analyzed by flow cytometry.

RNA isolation and real-time PCR

For the real-time PCR assay, granulocytes from CLP7d or Sham7d mice that were challenged with LPS or PBS for 3 h were lysed and stored in TRIzol reagent (Invitrogen, Thermo Fisher Scientific). Total RNA was processed according to the manufacturer's instructions. Isolated RNA was reverse-transcribed to cDNA using a High-Capacity cDNA Reverse Transcription Kit (Applied Biosystems, Thermo Fisher Scientific). Expression of mRNA encoding TNF-α, irak3, ptpn6 and socs1 was detected using the SYBR Green method, while NOS2, Arginase, CXCL1, CXCL2, CXCL3, CXCL5, CXCL7 and CCL2 mRNA were measured using the TaqMan method (ABI 7500 Real-Time PCR System, Applied Biosystems, Thermo Fisher Scientific). For all the measured genes, GAPDH was used as a housekeeping gene, and the relative mRNA expression of samples from non-stimulated, naive granulocytes (or others, as indicated in the figure legends) was used as a reference.

Western blotting

Purified granulocytes from the bone marrow of naive or CLP7d mice were cultured with and without 100 ng/mL LPS in RPMI 1640 with 10% FBS for time intervals up to 3 h. The cells were harvested and lysed with RIPA buffer containing PMSF and protease inhibitors. Total protein amounts were determined by a BCA assay (Invitrogen, Thermo Fisher Scientific, Waltham, Massachusetts, U.S.), and equal amounts of protein were loaded on precast 10% or 4–15% gels (Invitrogen, Thermo Fisher Scientific, Waltham, Massachusetts,

U.S.). After electrophoresis, proteins were transferred to a PVDF membrane, which was then blocked in 5% BSA. Antibodies against ERK, p38, p65 and their corresponding phosphorylated proteins, as well as antibodies against TNF, IRAK-M, SHP-1, SOCS-1 and β-actin, were incubated with membranes overnight at 4°C. Protein expression was visualized using a secondary antibody and an enhanced chemiluminescence (ECL) Western blotting substrate (Promega, Madison, WI). Images were taken using a ChemiDoc XRS+ System (Bio-Rad, Hercules, CA) following the manufacturer's instructions.

Library preparation of ATAC-seq

The granulocytes from Sham7d and CLP7d mice were stimulated with LPS or PBS *in vitro*, and were conducted to the ATAC-seq libraries preparation by the TruePrepTM DNA Library Prep Kit V2 for Illumina kit. In brief, 50,000 viable cells were used and collected by centrifugation at 500x g for 5min. The cells were resuspended in cold lysis buffer (10mM Tris-HCl, pH 7.4, 10mM NaCl, 3mM $MgCl_2$, 0.1% NP40 and 0.1% Tween 20) and incubated on ice for 10min. The pellets were collected by centrifugation at 500x g for 5min and resuspended with 50ul transposition mix (5x TTBL 10ul, TTE Mix V50 5ul, ddH_2O 35ul). Mixtures were incubated at 37°C for 30min and purified with AMPure XP. The recovered products were amplified using the index of TruePrepTM Index Kit V2 for Illumina and screened for fragment length with AMPure XP. The library was subjected to Illumina Nova-seq 6000 sequencing system in paired-end mode. Three independent experiments were performed in granulocytes per group.

ATAC-seq data analysis

All sequencing reads were aligned to the reference genome (mm10) with Bowtie2. Quality control were performed using fastQC v0.11.9 and fastp v0.23.2. Adaptors were trimmed with trimmomatic v0.39. Duplicate reads were flagged with Picard v 3.0.0–2. MACS3 v 3.0.0a7 were used to call peaks. Consensus peak regions across all sample were generated with bedtools intersect command with parameters '-e -f 0.5 -F 0.5'. Differentially accessible regions were determined with the DiffBind v3.11.0 R package, and read counts were normalized by reads in peaks. ATAC peak regions that show a change of mean ± 2x median absolute deviation and ≥2-fold changes (FDR <0.05) signal in pairwise comparisons were regarded as dynamic ATAC regions. Peaks were mapped to nearest genes with the ChIPseeker v1.37.0 package. KEGG pathway enrichement were performed with clusterProfiler v4.8.1 in R. To read coverage tracks of ATAC signals, we combined bam files from biological replicate samples, and created normalized bigWig files using samtools v1.12, and bamCoverage from deepTools v1.5.12 with parameters –scaleFactor and –normalizeUsing BPM. Read coverage tracks were displayed with IGV v2.16.0 and scaled by groups. Global changes in chromatin accessibility were plotted with computeMatrix and plotHeatmap from deepTools v1.5.12. The accession number for the raw data files of the ATAC sequencing analysis is NCBI SRA PRJNA994272.

Library preparation for CUT&RUN assays

In brief, the sort-purified cells (~1×10^5 cells for each replicate) were fixed with 1% formaldehyde for 10 min at room temperature and then suspended in RIPA buffer (10 mM Tris-HCl pH7.5, 1 mM EDTA, 150 mM NaCl, 0.2% SDS, 0.1% w/v sodium deoxycholate, and 1% Triton X-100) for nuclei extraction. The nuclei were then incubated with 0.5 μg rabbit anti-Histone H3 (dimethyl K4) antibody, rabbit anti-Histone H3 (acetyl K9) antibody, rabbit anti-Histone H3 (acetyl K27) antibody, or normal rabbit IgG in antibody-binding buffer (10 mM Tris-HCl pH7.5, 1 mM EDTA, 150 mM NaCl, and 1% Triton X-100) overnight with rotation. The unbound antibody was removed by washing the nucleus pellet with the Antibody-Binding buffer, and the nuclei were incubated with protein A/G-micrococcal nuclease (MNase) fusion protein for 1 h at 4°C. The unbound MNase was removed by washing with Wash buffer (10 mM Tris-HCl pH7.5, 1 mM EDTA, 400 mM NaCl, and 1% Triton X-100). After suspended in Resuspension buffer (20 mM Tris-HCl pH7.5, 10 mM NaCl, and 0.1% Triton X-100), the antibody-bound MNase was activated by addition of CaCl2 (final concentration 2 mM) followed by 30 min incubation at 0°C. The reaction was quenched with Stopping buffer (20 mM Tris,-HCl pH 8.0, 10 mM EGTA, 20 mM NaCl, 0.2% SDS, and 0.2 μg/μL proteinase K), and then incubated at 65°C for 2 h to reverse the crosslinking. The DNA fragments were purified with MinElute Reaction Cleanup kit, end-repaired, adaptor added and then amplified with PCR for 14 cycles with NEBNext Ultra II DNA Library Prep Kit for Illumina. The amplified DNA fragments were purified by AMPure XP beads. The library was subjected to Illumina Nova-seq 6000 sequencing system in paired-end mode.

CUT&RUN data analysis

Sequencing reads were aligned to the reference genome (mm10) with Bowtie2. Quality control were performed using fastQC v0.11.9 and fastp v0.23.2. Adaptors were trimmed with trimmomatic v0.39. Duplicate reads were flagged with Picard v 3.0.0–2. SEARCR v1.3 were used to call peaks. Analysis of coverage tracks for all histone modification signals were performed the same as those with ATAC-seq tracks as described above. Two independent experiments were performed in granulocytes per group. The accession number for the raw data files of the CUT&RUN assays is NCBI SRA PRJNA994272.

Chromatin immunoprecipitation (ChIP)

Isolated bone marrow granulocytes from Sham7d or CLP7d mice were stimulated with 100 ng/mL LPS for 3 h, fixed with 1% formaldehyde for 10 min and quenched in 125 mM glycine for 5 min. Fixed cells were lysed with ice-cold lysis buffer containing PMSF and a protease inhibitor cocktail (Sigma-Aldrich, St. Louis, MO). The chromatin was sonicated using a Bioruptor Plus (Diagenode, Denville, NJ) for 15 cycles of 30s on and 30 s off and was diluted with 1 mL dilution buffer with protease inhibitors. The unsonicated

chromatin lysate was used as the input control. The rest of the lysate was then incubated with H3K27Ac, H3K9ac, H3K4me2 or irrelevant (as a negative control) antibodies at 4°C overnight with constant rotation. Protein A/G Dynabeads (Thermo Fisher Scientific) suspended in ChIP dilution buffer containing 15 mg/mL BSA and 3 mg/mL tRNA were added to the mixture of chromatin and antibodies at 4°C for 90 min with rotation. Magnetic beads were washed successively with low salt, high salt and LiCl wash buffer and twice with Tris-EDTA buffer. Chromatin was then eluted with 250 μL elution buffer for 30 min. The reversal of cross-links was achieved by incubation at 65°C with 10 μL 5 M NaCl, 3 μL Proteinase K (20 mg/mL) and RNase A (10 mg/mL) for at least 4 h. DNA fragments were finally purified using a Chromatin IP DNA Purification Kit (Active Motif, Carlsbad CA). The purified DNA was analyzed using the SYBR Green method with the following primers: Irak3, 5′-CGTTCCTGCGGTGGTCATTACA-3' (forward primer) and 5′-AGGC CAAACCTGGGCAAACAAA-3' (reverse primer); Ptpn6, 5′-AGGGCTGGCAAGCAGAATTCAA-3' (forward primer) and 5′-TCAC CAGGGCCTCATTCCTCAG-3' (reverse primer); and Socs1, 5′-GTTCCAAGAAGGGTCGAGATTGC-3' (forward primer) and 5′-GCCCGCTCTTTTGCTCTACCT-3' (reverse primer). Percentages of each sample compared to the input were calculated as the amount of DNA fragments.

Metabolic flux assay

The real-time ECAR and OCR were measured using an XF96 extracellular flux analyzer (Seahorse Bioscience). Freshly isolated granulocytes (1×10^5 cells) were washed once in RPMI 1640 medium supplemented with 10% FBS and seeded in the corresponding assay medium in an XF plate coated with poly-L-lysine (Sigma). Cells were incubated for 1 h at 37°C before analysis. Two independent experiments were performed with six independent replicates per group.

RNA sequencing and bioinformatics analysis

Granulocytes from the bone marrow were lysed, and RNA was isolated using TRIzol reagent (Invitrogen). Only samples with an RNA integrity number (RIN) of 8 or higher, as measured using an Agilent Bioanalyzer 2100 (Santa Clara, CA, USA), were considered for further analysis. RNA samples were sequenced on an Illumina HiSeq 2500 platform (Illumina, San Diego, CA) according to the manufacturer's instructions. Briefly, sequencing libraries were generated using an NEBNext Ultra Directional RNA Library Prep Kit for Illumina (NEB, Ipswich, MA), and the clustering of index-coded samples was performed on a cBot Cluster Generation System using a TruSeq PE Cluster Kit v3-cBot-HS (Illumina, San Diego, CA) following the manufacturer's recommendations. Then, all library preparations were sequenced, and 100-bp paired-end reads were generated. The full datasets have been submitted to the NGDC (National Genomics Data Center) under accession number CRA001737.

RNA sequencing data were analyzed using the Tuxedo software package for transcript assembly,[49] gene expression level quantification and differential expression analysis. We trimmed the low-quality reads ($Q < 20$) and aligned the reads to the mouse genome (GRCm38) with HISAT.[50] These alignments were used to estimate transcriptomic alignment rates and expression levels. StringTie was used to assemble the alignments into full and partial transcripts,[51] and Ballgown was used to calculate the transcript expression level as the fragments per kilobase of exon per million reads mapped (FPKM).[52] Differentially expressed genes (DEGs) were defined as expression level changes of at least 4-fold between samples. The molecular functions (MF), BF and Kyoto Encyclopedia of Genes and Genomes (KEGG) pathway annotations and enrichment analysis for each gene were determined using an online tool, the Database for Annotation, Visualization and Integrated Discovery (DAVID).[53] GSEA analysis (another gene set enrichment analysis) were applied in R with cluster Profiler v3.10.1.[54]

ScRNAseq and bioinformatics analysis

Femurs and tibias were dissected after the sacrifice of the mice. Cells from the bone marrow were collected by rinsing the medullary cavity with phosphate buffered saline (PBS, Gibco, Thermo Fisher scientific). Then, 1×10^7 $CD11b^+$ myeloid cells were positively isolated with magnetic cell sorting according to manufacture instructions (Miltenyi Biotec), followed by culturing in RPMI 1640 medium supplemented with 10% FBS (R10, Gibico, Thermo Fisher Scientific) with or without 100 ng/ml LPS (Sigma) for 3 h (BD Biosciences). Four thousand cells were harvested and counted for single cell RNA sequencing. Single cell library was prepared according to the user guide of Single cell 3′reagent kits v2 (Chromium, 10X genomics). The libraries were sequenced one sample per lanes on a Hiseq X. The full datasets of the myeloid cells have been submitted to the NGDC (National Genomics Data Center) under accession number CRA001040, and the data files of the lung cells have been submitted to SRA (Sequence Read Archive, NCBI) under accession number PRJNA994272.

We analyzed the scRNAseq data with Seurat and Monocle R package.[55–57] The raw reads were then processed with Cell ranger software, where the sequencing reads were demultiplexing and barcode processing. The reads were aligned to mouse reference genome with STAR aligner.[58] The mapped reads were used for unique molecular identifier (UMI) counting and subsequent analysis to generate the expression matrix. The matrix of each sample was processed with Seurat R package for further analysis.[55,56] We removed batch effect and integrated four datasets with MNN algorism in Seurat. Then we cluster the cells with SNN algorism and then visualize the clusters with t Stochastic neighbor Embedding (tSNE). The marker genes in each cluster were identified with FindAllMarkers function. The pseudotime analysis and differential expression gene (DEG) identification were performed with Monocle package.[57] Pseudotime analysis were performed with reduceDimension function with DDRTree method. DEG genes were defined as expression level changes of at least 2-fold between samples and q-value less than 0.001.

QUANTIFICATION AND STATISTICAL ANALYSIS

All data were analyzed by using GraphPad Prism software (Version 7.0, GraphPad Software, La Jolla, CA). The normality of each variable was evaluated using the Kolmogorov-Smirnov test. For normally distributed data, a two-tailed Student's t test was performed to compare two variables, and one-way ANOVA was performed to compare more than two groups. The Mann-Whitney U test was used when data were not normally distributed. The log rank test was used to compare the survival rate between each group. Statistical parameters including the exact value of n, the statistical significance and dispersion measures are reported in the Figures and Figure Legends. A p value of <0.05 was considered significant.

Statistical analysis

All data were analyzed by using GraphPad Prism software (Version 7.0, GraphPad Software, La Jolla, CA). The normality of each variable was evaluated using the Kolmogorov-Smirnov test. For normally distributed data, a two-tailed Student's t test was performed to compare two variables, and one-way ANOVA was performed to compare more than two groups. The Mann-Whitney U test was used when data were not normally distributed. The log rank test was used to compare the survival rate between each group. Statistical parameters including the exact value of n, the statistical significance and dispersion measures are reported in the Figures and Figure Legends. A p value of <0.05 was considered significant.